

# A Pluto–Charon Sonata: The Dynamical Architecture of the Circumbinary Satellite System

Scott J. Kenyon

*Smithsonian Astrophysical Observatory, 60 Garden Street, Cambridge, MA 02138*

e-mail: skenyon@cfa.harvard.edu

Benjamin C. Bromley

*Department of Physics & Astronomy, University of Utah, 201 JFB, Salt Lake City, UT 84112*

e-mail: bromley@physics.utah.edu

## ABSTRACT

Using a large suite of  $n$ -body simulations, we explore the discovery space for new satellites in the Pluto–Charon system. For the adopted masses and orbits of the known satellites, there are few stable prograde or polar orbits with semimajor axes  $a \lesssim 1.1 a_H$ , where  $a_H$  is the semimajor axis of the outermost moon Hydra. Small moons with radii  $r \lesssim 2$  km and  $a \lesssim 1.1 a_H$  are ejected on time scales ranging from several yr to more than 10 Myr. Orbits with  $a \gtrsim 1.1 a_H$  are stable on time scales exceeding 100 Myr. Near-IR and mid-IR imaging with JWST and ground-based occultation campaigns with 2–3-m class telescopes can detect 1–2 km satellites outside the orbit of Hydra. Searches for these moons enable new constraints on the masses of the known satellites and on theories for circumbinary satellite formation.

*Subject headings:* planets and satellites: dynamical evolution and stability — planets and satellites: individual (Pluto)

## 1. INTRODUCTION

With four small satellites orbiting a binary planet, the Pluto-Charon system is a dynamical wonder (Weaver et al. 2006; Buie et al. 2006; Tholen et al. 2008; Showalter et al. 2011; Youdin et al. 2012; Buie et al. 2012; Showalter et al. 2012; Buie et al. 2013; Brozović

et al. 2015; Showalter & Hamilton 2015). The smallest satellite, Styx, lies reasonably close to the innermost stable orbit of the central binary. The larger satellites – Nix, Kerberos, and Hydra – are packed about as tightly as possible. Although the orbital periods of the satellites are almost integer multiples of the Pluto–Charon period, the satellites rotate chaotically on time scales much shorter than their orbital periods.

Spectacular images and spectroscopic data from the *New Horizons* flyby provide new insights (e.g., Bagenal et al. 2016; Grundy et al. 2016; Weaver et al. 2016; McKinnon et al. 2017; Robbins et al. 2017; Verbiscer et al. 2018; Lauer et al. 2018). The satellites are irregularly shaped, with equivalent spherical radii ranging from 10–12 km for Styx and Kerberos to 19–21 km for Nix and Hydra (see also Showalter & Hamilton 2015). Confirming earlier predictions (Youdin et al. 2012), albedos are large, ranging from roughly 55% for Kerberos and Nix to 65% for Styx to nearly 85% for Hydra. Thus, the surfaces of the satellites are much icier than Pluto or Charon (Cook et al. 2018). Expanding on the results of Showalter & Hamilton (2015), detailed analysis by the *New Horizons* team shows that the satellites are not tidally locked with the central binary; rotational periods range from 0.43 d for Hydra to 5.31 d for Kerberos.

Confounding theoretical expectations (e.g., Kenyon & Bromley 2014a; Bromley & Kenyon 2015b), *New Horizons* did not detect any new satellites. Data from a deep imaging survey place an upper limit on the radius,  $r \lesssim 1.7$  km, for smaller icy moons within 80,000 km ( $a \lesssim 1.23 a_H$ ) of the Pluto–Charon center-of-mass (Weaver et al. 2016). This result is a weak test of numerical simulations for satellite formation, which predicted several small satellites,  $r \lesssim 1$ –3 km, within 105,000 km of Pluto–Charon ( $a \approx 1.2 - 1.6 a_H$ ). The *New Horizons* data also place strong constraints on dusty debris orbiting Pluto–Charon in the vicinity of the known satellites (Bagenal et al. 2016; Lauer et al. 2018). The observed upper limit on the optical depth,  $\tau \lesssim 10^{-8}$  on  $10^3 - 10^4$  km scales, is well below early predictions of  $\tau \approx 10^{-7} - 10^{-5}$  (e.g., Stern et al. 2006; Steffl & Stern 2007; Poppe & Horányi 2011) but above more recent predictions of  $\tau \approx 10^{-11}$  (Pires dos Santos et al. 2013).

Without another Pluto–Charon flyby in the near future, placing additional constraints on the properties of the satellite system requires (i) more detailed analyses of existing data, (ii) expanded sets of numerical simulations, and (iii) new high quality observations from the ground or from a near-Earth telescope. In their discovery paper for Styx, Showalter et al. (2012) note that this moon is close to the detection limit for HST. Thus, it seems unlikely HST will find any fainter satellites (see also Steffl et al. 2006).

To isolate the possible discovery space for new satellites, we conduct an extensive series of  $n$ -body simulations. Our calculations follow the orbits of massive proxies for the four known satellites and sets of massless tracer particles orbiting a central binary with the

physical properties of Pluto–Charon. Adopting the masses in Table 1 and defining  $a_S$  ( $a_H$ ) as the semimajor axis of Styx (Hydra), our results demonstrate that nearly all test particles with initial semimajor axes  $0.95 a_S \lesssim a_0 \lesssim 1.1 a_H$  are unstable on time scales  $t \lesssim 10\text{--}20$  Myr. Test particles with the most stable orbits have  $a_0 \approx 0.85 - 0.93 a_S$  ( $a_0 \approx 36,000\text{--}40,000$  km) or  $a_0 \gtrsim 1.1 a_H$  ( $a_0 \gtrsim 75,000$  km).

Additional calculations show that massive satellites with radii  $r \lesssim 1\text{--}2$  km and mass density  $\rho \approx 1 \text{ g cm}^{-3}$  on orbits with  $a \gtrsim 75,000$  km are stable on  $100\text{--}150$  Myr time scales. In this semimajor axis range, polar and prograde orbits are comparably stable. Nearly all small moons with  $0.8 a_S \lesssim a_0 \lesssim 1.1 a_H$  are ejected on time scales ranging from a few yr to  $\sim 100\text{--}150$  Myr. Together with the calculations of massless tracers, these results clarify the most promising location for new satellites in the Pluto–Charon system: outside the orbit of Hydra.

We then consider two options for finding new satellites. With HST precluded, we show that (i) near-IR imaging with modest integration times on JWST instruments and (ii) occultations on medium-sized ground-based telescopes can track the orbits, shapes, and reflective properties of the known satellites and discover possible smaller satellites with high albedo and radii of  $1\text{--}2$  km.

After briefly describing the  $n$ -body code (§2.1) and the physical properties of the known satellites (§2.2), we consider the stability of circumbinary satellites in systems without and with the known Pluto–Charon satellites in §2.3–§2.5. We outline the observational programs in §3. We conclude with a brief discussion (§4) and summary (§5).

## 2. NUMERICAL SIMULATIONS

### 2.1. Background

To explore the extent of the plausible discovery space for new satellites in the Pluto–Charon system, we consider numerical simulations with *Orchestra*, a parallel C++/MPI hybrid coagulation +  $n$ -body code that follows the accretion, fragmentation, and orbital evolution of solid particles ranging in size from a few microns to thousands of km (Kenyon 2002; Bromley & Kenyon 2006; Kenyon & Bromley 2008; Bromley & Kenyon 2011a, 2013; Kenyon & Bromley 2016; Kenyon et al. 2016). The ensemble of codes within *Orchestra* includes a multi-annulus coagulation code, an  $n$ -body code, and radial diffusion codes for solids and gas. Several algorithms link the codes together, enabling each component to react to the evolution of other components.

Here, we use the  $n$ -body code to track the orbits of massive satellites and many massless tracers around the Pluto–Charon binary. For the satellites, we adopt the masses, radii, and orbital elements listed in Table 1 (Brozović et al. 2015; Showalter & Hamilton 2015; Weaver et al. 2016) and initial state vectors from Table 8 of Brozović et al. (2015). To derive the position and velocity of Pluto relative to the system barycenter, we adopt an orbital period of 6.387 d and  $m_P = 1.303 \times 10^{25}$  g,  $r_P = 1183$  km, and  $f_P \lesssim 0.006$  for the mass, radius, and oblateness of Pluto; Charon has mass  $m_C = 1.587 \times 10^{24}$  g =  $0.12 m_P$ , radius  $r_C = 606$  km =  $0.51 r_P$ , and oblateness  $f_C \lesssim 0.005$  (e.g., Young & Binzel 1994; Person et al. 2006; Brozović et al. 2015; Stern et al. 2015; Nimmo et al. 2017; McKinnon et al. 2017, and references therein). To simplify assigning orbits for massless tracer particles, we rotate the cartesian coordinate system of Brozović et al. (2015) to place the angular momentum vector  $L$  in the z-direction.

In this study, we do not consider how errors in the measured positions and velocities of Pluto–Charon and the smaller satellites might impact outcomes of the calculations. For a nominal distance of 40 AU from the Earth, a  $0''.01$  uncertainty in the centroid of the point spread function for a small satellite on an HST image corresponds to  $\sim 7$  km. Compared to the observed semimajor axes ( $4.2 \times 10^4 - 6.5 \times 10^5$  km) or the derived radii of their Hill spheres (200–700 km), this uncertainty is rather small. We performed several test calculations with initial positions differing by 5–10 km from the nominal positions for the small satellites. The results are identical to those starting from the nominal initial state vector. Thus, we consider results only for one initial state vector.

To evolve the ensemble of massless tracers, we place them on orbits with initial semimajor axis  $a$ ,  $e$ , and  $i$  relative to the binary center-of-mass. These orbits are similar to a set of ‘most circular’ circumbinary orbits with identical orbital elements (e.g., Lee & Peale 2006; Lithwick & Wu 2008b; Youdin et al. 2012; Leung & Lee 2013; Bromley & Kenyon 2015a,b, 2017). Adding circumbinary satellites to the Pluto–Charon binary limits the set of stable orbits for massless tracers (Lithwick & Wu 2008b; Youdin et al. 2012). Our goal is to find the set of stable tracer orbits for an adopted set of properties for the known satellites.

For each suite of simulations, we derive results using a symplectic integrator which divides the Pluto–Charon orbit into  $N$  steps and maintains a constant time step throughout the integration. As outlined in the Appendix, several tests demonstrate that a minimum  $N = 40$  enables calculations with negligible drift over 100–500 Myr in  $a$  and  $e$  for the Pluto–Charon binary and for small satellites with their nominal masses. The algorithm has also been verified with test simulations in previous papers (e.g., Duncan et al. 1998; Bromley & Kenyon 2006, 2011a,b, 2013, 2017).

On the NASA ‘discover’ computer system, we perform calculations on either 1 processor

(6-bodies or 7-bodies) or 56 processors (Pluto–Charon binary with massless tracers, with or without the small satellites). With 1 processor, a system with Pluto–Charon and the four known satellites evolves 4.2 Myr per cpu-day. Adding another small satellite reduces the evolution time to 3.0 Myr per cpu day. At these rates, completing a typical 100 Myr calculation requires 25–34 days. Multi-processor calculations with the central binary,  $56 \times 56 = 3136$  tracers, and the 4 small satellites complete 1.9 Myr of evolution per day. As the Pluto–Charon system ejects tracers, the calculations move somewhat faster. Typical 10–15 Myr calculations for these systems finish in 4–8 days.

For computational convenience, we perform calculations of tracers over a small range in semimajor axis  $a$ . When the small satellites are included, the range in  $a$  covers regions from (i) well inside to just outside the orbit of Styx, (ii) just inside the orbit of one of the small satellites to just outside the orbit of the next satellite with larger  $a$ , or (iii) just inside to well outside the orbit of Hydra. Instead of having a uniform density of tracers with  $a$ , this procedure generates an overlap of tracers co-rotating with each small satellite. Aside from allowing us to compare results for tracers with similar  $a$  from different calculations, these starting conditions provide a better measure of the survival rate for co-rotating tracers.

## 2.2. Physical Properties of the Pluto–Charon Satellites

To derive physical properties for the four small satellites (Table 1), we rely on published observations and  $n$ -body simulations. Orbital elements – the semimajor axis  $a$ , eccentricity  $e$ , inclination  $i$ , and orbital period  $P_{orb}$  – are from detailed analyses of HST imaging data (Brozović et al. 2015; Showalter & Hamilton 2015).

Comprehensive imaging data from HST and the *New Horizons* flyby demonstrate that all of the satellites have irregular, oblong shapes (Showalter & Hamilton 2015; Weaver et al. 2016). Aspect ratios are roughly 2:1:1 (Styx and Kerberos), 1.5:1:1 (Nix), or 3:2:1 (Hydra). For numerical simulations, we adopt equivalent spherical radii  $r_i = \sqrt[3]{x_i y_i z_i}$  where  $x_i$ ,  $y_i$ , and  $z_i$  are the three dimensions quoted in Weaver et al. (2016). The  $1\sigma$  errors in these radii are  $\pm 2.5$  km for Styx, Nix, and Kerberos and  $\pm 8.5$  km for Hydra.

Robust analyses of the HST imaging data yield satellite masses and  $1\sigma$  errors (in units of  $10^{18}$  g)  $m_S \lesssim 15$  (Styx),  $m_N = 45 \pm 40$  (Nix),  $m_K = 16.5 \pm 9$  (Kerberos), and  $m_H = 48 \pm 42$  (Hydra). Fits to the HST astrometry are rather insensitive to the masses of the small satellites (Brozović et al. 2015). Using the adopted radii, the satellites have mass density  $\rho_S \lesssim 25$  g cm $^{-3}$ ,  $\rho_N = 1.3 \pm 1.3$  g cm $^{-3}$ ,  $\rho_K = 18 \pm 10$  g cm $^{-3}$ , and  $\rho_H = 1.2 \pm 1.2$  g cm $^{-3}$ . Although the nominal densities for Nix and Hydra are reasonably close to the density of either

Charon ( $\rho_C = 1.70 \text{ g cm}^{-3}$ ) or Pluto ( $\rho_P = 1.85 \text{ g cm}^{-3}$ ), results for Styx and Kerberos are unphysical.

For the calculations in this paper, we adopt the HST masses for Nix and Hydra. Revising the mass density of Styx and Kerberos to the physically plausible  $\rho_S \approx \rho_K \approx 1 \text{ g cm}^{-3}$  yields masses,  $m_S = 0.6$  and  $m_K = 1$ , that are consistent with the detailed analyses of HST imaging data. Long-term  $n$ -body simulations with these masses yield stable systems over evolution times of 500 Myr. Test calculations show that doubling the adopted masses for Styx and Kerberos does not change the results significantly. We plan to investigate the masses of all of the satellites in more detail in a separate publication.

For massless tracers orbiting the Pluto–Charon binary with semimajor axes  $a_S \lesssim a \lesssim a_H$ , plausible regions of stability are set by the Hill radius

$$r_H = \left( \frac{m}{3 m_{PC}} \right)^{1/3} a, \quad (1)$$

where  $m$  is the mass of a satellite,  $m_{PC}$  is the combined mass of Pluto and Charon, and  $a$  is the semimajor axis of a nearby satellite. The fifth column of Table 1 lists the Hill radius of each satellite. In systems with several massive planets or satellites, massive objects typically clear out a zone with a half-width  $\delta a \approx K r_H$  around their orbits, with  $K = 8\text{--}10$  (e.g., Wisdom 1980; Petit & Henon 1986; Gladman 1993; Chambers et al. 1996; Deck et al. 2013; Fang & Margot 2013; Fabrycky et al. 2014; Mahajan & Wu 2014; Pu & Wu 2015; Morrison & Kratter 2016; Obertas et al. 2017; Weiss et al. 2018, and references therein).

Naive application of these constraints leave little space for satellites with  $a_S \lesssim a \lesssim a_H$ . Setting  $K \approx 10$  precludes other stable satellites between the orbits of Styx–Nix and Kerberos–Hydra, but allows moons in a small region  $a \approx 54,000\text{--}56,000 \text{ km}$  between the orbits of Nix and Kerberos. In terms of the binary separation  $a_{PC}$ , this stable region has  $a \approx 2.75\text{--}2.9 a_{PC}$ . The weaker constraint  $K \approx 8$  expands the stable region between Nix and Kerberos and enables a second stable region at  $a \approx 2.22\text{--}2.27 a_{PC}$  (43,500–44,500 km) between the orbits of Styx and Nix. Stable satellites between the orbits of Kerberos and Hydra are still prohibited.

The Hill condition also allows stable satellites with  $a \approx 1.84\text{--}2.15 a_{PC}$  inside the orbit of Styx and  $a \gtrsim 3.75 a_{PC}$  beyond the orbit of Hydra. For  $a \lesssim 2.15 a_{PC}$ , it seems likely that the Pluto–Charon binary, Nix, and Hydra will eventually drive out massive satellites. Far outside the orbit of Hydra ( $a \gtrsim 50 a_{PC}$ ), the gravity of Hydra, the Sun, and the major planets combine to preclude stable satellites for some range of  $a$ ,  $e$  and  $i$  (Michaely et al. 2017). Inside this region, orbits are generally stable. Although some orbits with  $a \approx 1.84\text{--}2.15 a_{PC}$  might be stable, we expect satellites with  $a \gtrsim 3.75 a_{PC}$  are stable on longer time scales.

### 2.3. Stability of Tracers in Circumbinary Orbits

Although there have been many studies of the stability of circumbinary orbits (e.g., Dvorak et al. 1989; Holman & Wiegert 1999; Pilat-Lohinger et al. 2003; Pichardo et al. 2005; Musielak et al. 2005; Pichardo et al. 2008; Verrier & Evans 2009; Farago & Laskar 2010; Doolin & Blundell 2011; Li et al. 2016), only a few results are generally applicable to the Pluto–Charon binary (see also Youdin et al. 2012, and references therein). Nearly all orbits with  $a \gtrsim 3 a_{PC}$  are stable. For co-planar, prograde circumbinary satellites with inclination  $i \approx 0^\circ$  orbiting a Pluto–Charon binary with  $e_{PC} \lesssim 5 \times 10^{-5}$  (Brozović et al. 2015), the innermost stable orbit has a semimajor axis  $a_0 \approx 1.7\text{--}2 a_{PC}$ . Some retrograde orbits ( $i \approx \pi$ ) with  $a \approx 1\text{--}2 a_{PC}$  are stable (Doolin & Blundell 2011). Although orbits with  $a \approx 1\text{--}3 a_{PC}$  and  $i \gg 0^\circ$  are generally less stable than their  $i \approx 0^\circ$  counterparts, there are islands of stability with  $a \approx 1\text{--}2 a_{PC}$  and some  $i$ .

To identify plausible locations for small circumbinary satellites in the current Pluto–Charon system, we follow sets of massless test particles orbiting the Pluto–Charon binary. In these initial tests, we do not include the four small satellites. Rather than attempt to duplicate previous efforts in complete detail (e.g., Doolin & Blundell 2011), our goal is to locate stable regions for prograde/retrograde orbits with small inclination to the orbital plane of the binary and for polar orbits with initial  $i \approx 90^\circ$ . To facilitate this goal, we define a ‘survivor fraction’ as the fraction of tracers in orbit after 1–2 Myr of evolution,  $f_s = N_s/N_0$ , where  $N_s$  is the number of survivors and  $N_0$  is the initial number of tracers. Table 2 summarizes  $f_s$  for these calculations.

For the first tests, we examine calculations of the orbital evolution of massless tracers with initial eccentricity  $e_0 = 10^{-5}$  and a range of semimajor axes,  $a_0 = 1.0\text{--}1.5 a_{PC}$  and  $a_0 = 1.45\text{--}2.1 a_{PC}$ , on prograde ( $i \approx 0$ ), polar ( $i \approx \pi/2$ ), and retrograde ( $i \approx \pi$ ) orbits. Because we do not mix tracers with different inclinations, these tests require six distinct calculations with 3136 tracers in each calculation. Within this set, only one tracer on polar orbits survives. A comparison of the orbital evolution of this tracer with others on polar orbits suggests it will be ejected in  $\lesssim 1$  Myr. Thus  $f_s = 0$  for polar orbits with  $a_0 = 1.0\text{--}2.1 a_{PC}$ . Among tracers on prograde orbits, none with  $a_0 = 1.0\text{--}1.5 a_{PC}$  survive; however, 29% of those with  $a_0 \approx 1.45\text{--}2.1 a_{PC}$  remain. Tracers on retrograde orbits are more stable: 20% (98%) of the survivors have  $a_0 = 1.0\text{--}1.5 a_{PC}$  (1.45–2.1  $a_{PC}$ ).

Fig. 1 shows the distribution of  $a$  and  $e$  for particles that survive for 1–2 Myr. The lone polar survivor has  $a \approx 2.05 a_{PC}$  and  $e \approx 0.04$ . Among prograde tracers, survivors have  $a \gtrsim 1.70\text{--}1.75 a_{PC}$  and  $e \approx 0.01\text{--}0.1$ . Most are concentrated in a cloud with  $a \approx 2 a_{PC}$  and  $e \approx 0.03$ . Retrograde survivors have  $a \gtrsim 1.3 a_{PC}$ ; the typical  $e$  ranges from roughly 0.1 at  $a \approx 1.4 a_{PC}$  to 0.01 at  $a \approx 2.1 a_{PC}$ .

Tracers with larger  $a_0$  are more likely to survive. When  $a_0 = 1.95\text{--}2.65 a_{PC}$  ( $a_0 = 2.60\text{--}3.25 a_{PC}$ ), roughly 2% (10%) on polar orbits survive for 1–2 Myr (Table 2). The survivor fraction is much larger for tracers on prograde orbits – 90% for  $a_0 = 1.95\text{--}2.65 a_{PC}$  and 100% for  $a_0 = 2.60\text{--}3.25 a_{PC}$ . All of the retrograde tracers survive,

Fig. 2 shows  $(a, e)$  for survivors with  $a_0 = 1.95\text{--}3.25 a_{PC}$ . Prograde and retrograde tracers have a clear trend in  $e(a)$ , with  $e \approx 0.01\text{--}0.1$  at  $a \approx 2 a_{PC}$  and  $e \approx 0.001\text{--}0.01$  at  $a \approx 3.2 a_{PC}$ . Sets of polar tracers have little or no trend in  $e$  with  $a$ . However, there is an abrupt inner edge to the distribution of polar tracers at  $a \approx 2.2$  apc. For all sets of tracers, there is a broad range of  $e$  at every stable  $a$ .

The minimum semimajor axes for circumbinary particles –  $a_c/a_{PC} \approx 1.7$  for prograde tracers, 2.2 for polar tracers, and 1.30–1.35 for retrograde tracers – agree with previous results. For example, Doolin & Blundell (2011) infer  $a_c/a_{PC} \approx 1.75$  (prograde), 2.2 (polar) and 1.3 (retrograde). The Holman & Wiegert (1999) fit to a suite of simulations yields  $a_c/a_{PC} \approx 2$  for prograde orbits; retrograde orbits have a smaller  $a_c$  (Wiegert & Holman 1997). The somewhat larger  $a_c$  for prograde orbits from Holman & Wiegert (1999) matches the location of the high density cloud of survivors in Fig. 1. Given the smaller number of simulations with shorter duration performed by Holman & Wiegert (1999), it is possible that their calculations identified the most likely  $a_c$  rather than the true  $a_c$ .

#### 2.4. Stability of Tracers in Circumbinary Orbits with Massive Satellites

We now consider the stability of tracers in systems with Pluto-Charon and the four small satellites. The state vector of Brozović et al. (2015) establishes initial positions and velocities of Pluto-Charon, Styx, Nix, Kerberos, and Hydra. For simplicity, we transform the coordinates to a cartesian system where the orbital plane of Pluto-Charon defines  $z = 0$ . Tracers begin on nearly circular ( $e_0 \approx 10^{-5}$ ) prograde orbits with low ( $i \approx 10^{-5}$ ) or high ( $i \approx \pi/2$ ) inclination. For three sets of calculations, the initial semimajor axis of each tracer is randomly distributed between  $0.975 a_i$  and  $1.025 a_{i+1}$  where  $i$  is 1 (Styx), 2 (Nix), 3 (Kerberos), and 4 (Hydra). In a fourth (fifth) calculation, tracers have initial semimajor axes ranging from  $0.7 a_S$  to  $1.025 a_S$  ( $0.975 a_H$  to  $1.125 a_H$ ). The  $n$ -body code follows the orbits of tracers until all have been ejected or for 10 Myr.

Among massless tracers on prograde orbits inside the orbit of Styx, roughly 20% survive 10 Myr of dynamical evolution. In the first year, nearly half are ejected; less than a third remain after 0.5 Myr. At the end of the evolutionary sequence, the system ejects a few tracers per Myr. If this rate is maintained indefinitely, all would be ejected in 100–200 Myr.

It seems likely that the rate will slow; thus, some are likely to survive for several Gyr.

The survival rate for tracers placed on prograde orbits outside the orbit of Styx and inside the orbit of Hydra is much smaller (Table 2). During the first Myr, nearly 90% are ejected. Over the next 9 Myr, the ejection rate slows considerably and eventually falls to roughly 1–2 tracers per Myr. After 10 Myr, the survival fractions are  $f_s = 0.02$  (Styx–Nix tracers), 0.004 (Nix–Kerberos tracers), and 0.02 (Kerberos–Hydra tracers). Over the next 100–200 Myr, the small but finite removal rate during the first 10 Myr implies the removal of all tracers initially placed inside the orbit of Hydra.

Tracers starting from just inside the orbit of Hydra to roughly  $1.2a_H$  have a larger survival rate. During the first 1–2 Myr of evolution, Nix and Hydra eject nearly half of the tracers. After this initial flurry, the ejection rate slows to a trickle. At 10 Myr,  $f_s = 0.45$ .

For prograde tracers, the distributions of  $(a, e)$  show several clear features. Inside the orbit of Styx, the density of survivors peaks at 1.8–2.0  $a_{PC}$  (Fig. 3). Within the corotation zones of Nix and Hydra, a few tracers orbit with  $e = 0.005$ –0.05 (Fig. 4–5). There are essentially no tracers outside any of the corotation zones or in the corotation zones of Styx and Kerberos. Survivors also have a strong concentration outside the orbit of Hydra, extending over a region bounded by  $a \approx 3.6 - 4.0 a_{PC}$  and  $e \approx 10^{-4} - 10^{-1}$ , with a strong density maximum at  $(a, e) \approx (3.8 a_{PC}, 0.005)$ .

Among tracers in the corotation zones of Nix and Hydra, the evolution of  $e$  follows a standard pattern. For several Myr,  $e$  gradually grows from  $\lesssim 0.001$  to 0.05. At some point, perturbations by the central binary, Nix, and Hydra generate  $e \gtrsim 0.05$  and the tracer begins to cross the orbit of either Nix or Hydra. After another few thousand years, the tracer leaves the system.

Within the strong concentration of tracers inside the orbit of Styx and outside the orbit of Hydra,  $e$  traces a similar evolution. Tracers that achieve  $e \gtrsim 0.02$  suffer small oscillations in  $a$  and an increasingly larger  $e$  until the pericenter of their orbit approaches the orbit of Styx/Nix (tracers originally inside the orbit of Styx) or Hydra (tracers originally outside the orbit of Hydra). The gravity of either Nix or Hydra then ejects them from the system. The upper envelope of the cyan points in the upper right corner of Fig. 5 show the clear growth of  $e$  with increasing  $a$  that characterizes dynamical ejections (see also Duncan & Levison 1997; Gladman et al. 2002).

The evolution of polar tracers is somewhat different. Unlike prograde tracers, polar tracers with orbits that cross within the corotation zone of a massive satellite are rapidly ejected from the system. Tracers with orbits that cross between the satellites are harder to remove. These tracers spend most of their time well outside the ‘clearing zone’ of the

massive satellites and take somewhat longer to eject. Still, some regions are cleared rapidly: it takes only 50 kyr to eject 100% (90%) of polar tracers with initial semimajor axes inside the orbit of Styx (between the orbits of Styx and Nix). Despite the slow removal rate for tracers inside the orbit of Nix after 0.1 Myr, all are lost after 6 Myr.

Polar tracers survive more easily outside the orbit of Nix (Table 2). For orbits between Nix–Kerberos (Kerberos–Hydra), it takes 0.1 Myr (0.3 Myr) to reduce the initial number of tracers by 50%. The removal rate then slows considerably. After 10 Myr, the survivor fractions are  $f_s = 0.21$  (Nix–Kerberos tracers) and  $f_s = 0.14$  (Kerberos–Hydra tracers). To examine the removal rate at later times, we extended these calculations to 20 Myr. At this point the survivor fractions have dropped to  $f_s = 0.18$  (Nix–Kerberos) and  $f_s = 0.08$  (Kerberos–Hydra). In both cases, the removal rate at 20 Myr suggests that the Pluto–Charon satellite system will eventually eject all of the tracers with polar orbits between Nix and Hydra, on a time scale of  $\sim 50$  Myr for Nix–Kerberos tracers and  $\sim 30$  Myr for Kerberos–Hydra tracers.

The longer lifetime for polar tracers between the orbits of Nix and Kerberos is due to the larger Hill spacing factor ( $K = 16$ ) relative to the  $K = 10$  factor for the Kerberos–Hydra pair. With Hydra’s larger nominal mass and its closer orbit to Kerberos, the volume available for extra satellites is much larger between Nix and Kerberos than it is between Kerberos and Hydra. The larger (smaller) volume results in a slower (faster) removal process for tracers on unstable orbits between Nix and Kerberos (Kerberos and Hydra).

Outside the orbit of Hydra, tracers on polar orbits are much more stable. After 1 Myr (3 Myr), the massive satellites have ejected only 30% (36%) of tracers on polar orbits with  $a_0 = 3.2\text{--}4.0 a_{PC}$ . After 20 Myr, the survivor fraction exceeds 0.5 (Table 2). Based on the slow rate of removal for this set of polar tracers, many will survive for  $\gtrsim 500$  Myr.

Despite differences in the dynamical evolution between tracers on polar orbits and tracers on low inclination prograde orbits, the distributions of  $(a, e)$  have some common features (Figs. 6–7). At any time, the range in  $e$  for survivors is very large with a maximum  $e$  of roughly 0.05 for prograde orbits and roughly 0.01 for polar orbits. Tracers excited to larger  $e$  are rapidly ejected. In both sets of calculations, dynamical evolution generates a dense cloud of tracers with  $(a, e) \approx (3.8 a_{PC}, 0.05)$ . Within this cloud, the maximum stable  $e$  is 0.01–0.02 instead of 0.05–0.10.

To conclude this section, Figs. 8 and 9 display the configuration of tracers within the Pluto–Charon satellite system after 10 Myr. Animations associated with each figure illustrate the time evolution of the complete population. Because we calculate the evolution of tracers in bands that overlap each satellite, the overall population of tracers is somewhat larger

along the orbit of each satellite than in the volume between the satellites.

For the ensemble of prograde tracers, it takes 100–300 yr for Nix and Hydra to begin clearing out particles along their orbits. Slight density maxima appear along the orbits of the lower mass satellites. Over roughly 3000 yr, Nix nearly clears out material in its Hill volume, except for a narrow co-rotation zone. With a longer orbital period, Hydra clears out a similar region in 10–30 kyr. During this period, the satellites eject tracers in the density maxima along the orbits of Styx and Kerberos. As the evolution proceeds, the satellites clear out the Hill volumes of Styx and Kerberos (including their co-rotation zones), while Nix and Hydra continue to work on removing tracers inside their co-rotation zones (0.1–0.3 Myr). Once the evolutionary sequence is complete, there are large sets of tracers just inside the orbit of Styx and just outside the orbit of Hydra, along with a few tracers in the co-rotation zones of Nix and Hydra. Otherwise, the system is fairly empty (Fig. 8).

The evolution of polar tracers shows several contrasting features (Fig. 9 and associated animation). Without the four circumbinary satellites, polar tracers inside the orbit of Styx are unstable (Fig. 1). Nearly all of these tracers disappear within 1000 yr. As the binary ejects these tracers, Nix and then Hydra begin to clear polar tracers that intersect their orbits. Unlike systems of prograde tracers in the orbital plane of the binary, polar tracers orbiting in the co-rotation zones of each satellite are ejected as rapidly as other tracers within the Hill volume. After 10 kyr (100 kyr), the Hill volume of Nix (Hydra) is nearly empty. As Nix completes clearing its Hill volume, the central binary ejects the last few tracers inside the orbit of Styx; Kerberos also begins to eliminate tracers from its orbit. At 1 Myr, the volume inside the orbit of Nix and the Hill volumes of Kerberos and Hydra are nearly devoid of tracers. After 10–20 Myr, many tracers remain between the orbits of Nix–Kerberos and Kerberos–Hydra and well outside the orbit of Hydra.

As the Pluto–Charon binary and small satellites clear polar tracers out of the corotation zones and the region inside the orbit of Nix, they also clear out material near the 9:2 resonance with the orbit of the central binary. Visible as a narrow dark band in the positions of tracers between the orbits of Nix and Kerberos in Fig. 9, the density of tracers in this region is roughly 60% of the density in the rest of this group. The outer edge of the distribution of tracers between the orbits of Kerberos and Hydra is close to the 11:2 resonance. However, there are no tracers between this resonance and the orbit of Hydra. Outside the orbit of Hydra, there is another drop in density at the 7:1 resonance with the binary. This drop is not visible as a dark band in Fig. 9; yet, the density of particles is roughly 70% of the density in the rest of the group outside the orbit of Hydra. Although our calculations did not examine the evolution of polar tracers with more distant orbits, the central binary and the small satellites remove polar tracers at the  $n:1$  resonances (with  $n = 2-7$ ) or the  $n:2$

resonances (with  $n = 3, 5, 7, 9, 11,$  and  $13$ ) on time scales of  $\lesssim 1\text{--}10$  Myr.

## 2.5. Stability of Low Mass Satellites

Although the calculations with massless tracers establish likely locations for small particles in the Pluto–Charon system, they do not allow us to constrain sets of stable orbits for small satellites with mass. To test whether massive satellites can have as long lifetimes as massless tracers, we select a group of massless, prograde test particles that have survived 10 Myr of circumbinary evolution (Figs. 3–5), assign each a radius of 2 km and a mass of  $4 \times 10^{16}$  g ( $\rho_s = 1.2$  g cm $^{-3}$ ), and evolve them with Pluto–Charon, Styx, Nix, Kerberos, and Hydra. To avoid gravitational interactions among the survivors, we follow the evolution of only one survivor in addition to the central binary and the four known satellites of Pluto–Charon.

For each set of survivors, the lifetime as a massive satellite is a strong function of initial conditions (Table 2; Fig. 10). Among those with orbits inside the orbit of Styx (near the corotation zone of Nix), survival times range from 1 yr to  $\sim 100$  Myr (30 yr to  $\gtrsim 100$  Myr). Satellites starting within the corotation zone of Hydra last somewhat longer, from roughly 20 kyr to  $\gtrsim 100$  Myr. Despite the large range in lifetimes, 90% of the satellites initially inside the orbit of Styx and near the corotation zone of Nix are ejected within 100 Myr; 79% of satellites initially near the corotation zone of Hydra are ejected after 100 Myr. To examine the survival rate at later times, we extended calculations for survivors to 150 Myr. At this point, the survivor fractions are  $f_s = 0.10$  (satellites inside the orbit of Styx), 0.10 (satellites co-rotating with Nix), and 0.14 (satellites co-rotating with Hydra). Based on the gradual increase in  $e$  and  $i$  for these survivors at 100–150 Myr, the likelihood that 2 km satellites inside the orbit of Hydra survive for the age of the solar system is small.

Massive moons on prograde orbits outside the orbit of Hydra are stable. After 100 Myr of circumbinary evolution,  $\sim 3.5\%$  of the satellites are ejected. Another 7% are ejected after 150 Myr. For each surviving satellite, there are no obvious trends in the evolution of  $a$ ,  $e$ , or  $i$ . Although it is possible that the orbits of some satellites might suffer significant perturbations at later times, the long lifetimes of these moons suggests that many are stable on 4–5 Gyr time scales.

To investigate the potential for small moons on polar orbits, we select a group of tracers that survive 10–20 Myr of evolution on polar orbits among the known Pluto–Charon satellites (Figs. 6–7). As with prograde moons, we assign each a radius of 2 km and evolve each one together with the known satellites. Because polar tracers do not survive inside the orbit of

Nix, we only consider the evolution of small moons between the orbits of Nix–Kerberos and Kerberos–Hydra and outside the orbit of Hydra.

Between the orbits of Nix–Kerberos and Kerberos–Hydra, several small moons survive 100 Myr of dynamical evolution (Table 2; Fig. 11). Moons orbiting between Nix and Kerberos often have short lifetimes of 1–10 kyr; others survive for less than 1 Myr. Roughly 21% complete a 100 Myr calculation on a stable orbit. With a minimum lifetime of roughly 1 Myr, moons on polar orbits between Kerberos and Hydra generally last somewhat longer. However, few survive for 10 Myr. After 100 Myr, only  $\sim 3.5\%$  are still on fairly stable orbits.

Outside the orbit of Hydra, small moons on polar orbits generally survive for 100 Myr. For these satellites, perturbations from the known moons are fairly small. Orbiting well inside the Pluto–Charon Hill sphere, these satellites are also fairly immune to jostling from the giant planets and other passersby. As with small moons on prograde orbits outside the orbit of Hydra, we expect that many of these can survive for  $\gtrsim 1$  Gyr.

## 2.6. Summary

Direct  $n$ -body simulations of circumbinary satellites confirm previous conclusions for the semimajor axis of the innermost stable orbit (e.g., Doolin & Blundell 2011). Massless prograde (retrograde) satellites with small  $i$  relative to the plane of the binary orbit are unstable when the initial semimajor axis  $a_0 \lesssim 2.1 a_{PC}$  ( $a_0 \lesssim 1.7 a_{PC}$ ). Stable satellites on polar orbits must have  $a_0 \gtrsim 2.2 a_{PC}$ .

For the adopted masses of Styx, Nix, Kerberos, and Hydra, possible orbits for other stable satellites are tightly constrained. On time scales ranging from a few yr to 10 Myr, nearly all massless tracers with prograde or polar orbits and  $0.95 a_S \lesssim a \lesssim 1.1 a_H$  are ejected. Survivors on prograde orbits lie well inside the orbit of Styx or within the corotation zones of Nix and Hydra. Despite the lack of polar survivors inside the orbit of Nix, some tracers remain on orbits between Nix–Kerberos or Kerberos–Hydra. Based on the time evolution of  $e$  and the loss rate at 5–20 Myr, we suspect nearly all will be ejected within 100 Myr. For prograde and polar orbits, many tracers outside the orbit of Hydra ( $a \approx 3.6$ – $4.0 a_{PC}$ ) are stable on  $\gtrsim 10$  Myr time scales. The orbital evolution of these tracers suggests they will remain stable over Gyr time scales.

Experiments with massive satellites confirm these conclusions. Moons with radius  $r = 2$  km and mass  $m = 4 \times 10^{16}$  g on prograde orbits with initial semimajor axis  $a_0 \approx 1.7$ – $2.1 a_{PC}$  are unstable on time scales ranging from a few yr to 100–150 Myr. Prograde satellites corotating in the orbits of Nix or Hydra are ejected on time scales of 30 yr to

150 Myr. Small moons outside the orbit of Hydra ( $a \approx 75,000$  km to 80,000 km) survive for 150 Myr and are likely on stable orbits.

Small moons on polar orbits also survive 100 Myr of dynamical evolution. Among those with  $a_0$  between the orbits of Nix–Kerberos (Kerberos–Hydra), a few remain on stable orbits. However, nearly all are ejected. Satellites with polar orbits beyond Hydra are generally stable.

These results agree with expectations based on the Hill radius of each satellite. From previous calculations of multi-planet or multi-satellite systems orbiting single or binary central objects, stability requires  $K \gtrsim 8$ –10 (e.g., Wisdom 1980; Petit & Henon 1986; Gladman 1993; Chambers et al. 1996; Deck et al. 2013; Fang & Margot 2013; Fabrycky et al. 2014; Mahajan & Wu 2014; Pu & Wu 2015; Morrison & Kratter 2016; Obertas et al. 2017). With no stable tracers between the orbits of Styx and Hydra, our calculations support the more conservative  $K \gtrsim 10$ .

The conservative limit for satellite stability disagrees with results from Porter & Stern (2015), who predicted stable locations for satellites prior to the *New Horizons* flyby. After re-analyzing HST data and suggesting a somewhat smaller (larger) mass for Nix (Hydra), they describe a suite of numerical calculations which indicate a broad range of stable orbits for particles between the orbits of each pair of satellites. Formally, these results imply  $K \lesssim 2$ –3. With typical durations of 1700 yr, however, their integrations are too short to infer robust lifetimes for extra satellites in the Pluto–Charon system (e.g., Youdin et al. 2012). Although *Orchestra* calculations confirm a large survivor fraction for tracers with  $a_S \lesssim a_0 \lesssim a_H$  at 1000–3000 yr (see the animations associated with Figs. 8–9), longer-term calculations demonstrate that particles with  $0.95 a_S \lesssim a_0 \lesssim 1.1 a_H$  are ejected on a broad range of time scales that are often much larger than a few thousand years (see also Youdin et al. 2012). Based on these longer integrations, we conclude that stable orbits with  $a_S \lesssim a \lesssim a_H$  for additional satellites are rare.

### 3. OBSERVATIONAL PROGRAMS

To construct observational programs to detect new satellites and to improve constraints on the known Pluto–Charon satellites, we adopt the nominal satellite properties in Table 1. At a distance from the Earth of roughly 40 AU ( $6 \times 10^{14}$  cm), Hydra is  $2''$  away from Pluto. Styx is somewhat closer, at an angular distance of  $1''3$ . The circumference of Hydra’s (Styx’s) orbit is  $12''5$  ( $8''$ ); during its 38 d (20 d) orbital period, Hydra (Styx) moves an arcsec every 3.33 d (2.52 d), equivalent to 0.01 (0.0075) arcsec per hr. From the standpoint of telescopic

observations over several hours, Hydra, Styx, and the other satellites are effectively stationary with respect to Pluto.

### 3.1. Direct Imaging with JWST

To explore options for detecting Pluto–Charon satellites with JWST, we rely on published descriptions of the instruments (e.g., Beichman et al. 2012; Doyon et al. 2012; Rieke et al. 2015) and sensitivity estimates from the *JWST Pocket Guide*<sup>1</sup>. With fields-of-view ranging from  $74'' \times 113''$  (MIRI; the Mid-Infrared Instrument) to  $2'.2 \times 2'.2$  (NIRISS; Near-Infrared Imager and Slitless Spectrograph) to  $2 \times 2'.2 \times 2'.2$  (NIRCam; Near-Infrared Camera), all of the JWST instruments can probe satellites well outside Hydra’s orbit. Although each instrument has tools to mask out part of the field, MIRI is not sensitive enough to detect Nix or Hydra at  $10 \mu\text{m}$  (see below). NIRCam and NIRISS have complementary masking options and similar sensitivity for K-band imaging, with  $10\sigma$  detections of 10 nJy sources expected in exposure times of  $10^4$  s.

Among the known satellites, Nix and Hydra have  $V = 23\text{--}24$  and equivalent spherical radii of roughly 20 km. Adopting optical/infrared colors of the Sun for these high albedo objects ( $V\text{--}K = 1.5$ ; Weaver et al. 2016),  $K \approx 22$ . For point sources having a flux of roughly  $10^3$  nJy, a 100 s integration with a JWST imager yields a  $10\sigma$  detection. With  $V = 26\text{--}27$  and  $K \approx 25$ , the smaller Styx and Kerberos require a factor of 10–20 longer integration time for a  $10\sigma$  detection.

If Nix and Hydra have the mid-IR colors of the Sun, we expect  $5 \mu\text{m}$  ( $10 \mu\text{m}$ ) fluxes of 200 nJy (60 nJy). At their long-wavelength cutoffs of roughly  $4.5 \mu\text{m}$ , NIRCam and NIRISS can achieve  $S/N = 10$  detections in 200 s integrations. Using MIRI, we expect  $S/N = 10$  (3) detections of Nix or Hydra with  $10^4$  s integration times at  $5 \mu\text{m}$  ( $10 \mu\text{m}$ ). MIRI’s coronagraph is unavailable at  $5 \mu\text{m}$ ; high quality detections at  $10 \mu\text{m}$  require much longer integration times than shorter wavelength observations with either NIRCam or NIRISS.

If there are any 1–2 km high albedo satellites in the Pluto–Charon system, they are 100–200 times fainter than Nix/Hydra. Integrations which yield  $10\sigma$  detections of Styx and Kerberos result in  $3\sigma$  detections for these putative satellites. Longer integrations improve the likelihood of identifying any 1–2 km satellites in the system.

Overall, detecting the known satellites of Pluto–Charon with JWST is straightforward. A program that acquires 5–10  $10^3$  sec integrations yields excellent  $S/N$  for Nix/Hydra, very

---

<sup>1</sup>e.g., the ‘Pocket Guide’ at <https://jwst.stsci.edu/instrumentation/miri>

good S/N for Kerberos/Styx, and sufficient S/N to detect 1–2 km objects from the orbit of Styx to well outside the orbit of Hydra.

### 3.2. Occultations

The Pluto–Charon system has a long and distinguished history of stellar occultation observations (e.g., Person et al. 2013; Boissel et al. 2014; Gulbis et al. 2015; Bosh et al. 2015; Pasachoff et al. 2016, 2017, and references therein). Aside from demonstrating the presence of Pluto’s atmosphere (Elliot et al. 1989) and measuring physical conditions within the atmosphere (e.g., Hubbard et al. 1988; Elliot et al. 2003; Pasachoff et al. 2005), data from occultations provide detailed astrometry on the Pluto–Charon orbit, the ephemerides of the Pluto–Charon system, and information on dust and other small objects orbiting Pluto–Charon. Although Charon has been probed with occultations (e.g., Gulbis et al. 2015), the lone published attempt to monitor an occultation by Nix did not yield the expected drop in stellar flux (Pasachoff et al. 2016).

For the Pluto–Charon system with a semimajor axis  $a \approx 40$  AU, occultations of small satellites with  $r \approx 1$ –2 km are in the Fresnel limit (e.g., Bailey 1976; Cooray & Farmer 2003; Roques et al. 2006; Nihei et al. 2007; Bickerton et al. 2008; Wang et al. 2009; Schlichting et al. 2009, 2012, and references therein). On this scale, the duration of an occultation is

$$\Delta t = 2D\phi_\star(1 + A^{1/2})/v \quad (2)$$

where  $D$  is the distance from the Earth to Pluto,  $\phi_\star$  is the angular size of the occulted star,  $v$  is the relative velocity, and  $A = (r/R_\star)^2$  is the amplitude of the occultation. In the amplitude,  $r$  is the radius of the satellite and  $R_\star = D\phi_\star$  is the projected size of the star at Pluto.

Achieving a large amplitude requires that the projected size of the star is comparable to the radius of the satellite. With  $R_\star = 1$ –10 km and  $D = 40$  AU,  $\phi_\star \approx 2 - 20 \times 10^{-10}$ . If the physical radius of the star is similar to the solar radius, the distance to the star is  $d \approx 10$ –100 pc.

Although the amplitude of the occultation can be large, the duration is very short. For a 1 km (10 km) satellite with  $R_\star = 1$  km, Pluto’s orbital motion of  $v = 5$  km s<sup>−1</sup> implies  $\Delta t = 0.8$  s (8 s). Resolving the event requires integration times of 0.04 s (0.4 s). The relatively long duration of occultations of 10–20 km satellites makes the event much easier to resolve than occultations by 1–2 km satellites.

Relaxing our assumption of spherical satellites makes occultation observations somewhat

more challenging. From *New Horizons* data, the aspect ratios range from roughly 1.5:1:1 for Nix to roughly 2:1:1 for Styx and Kerberos to roughly 2.6:1.8:1 for Hydra. For a worst-case where long axis of the satellite lies perpendicular to its path across the star, it is prudent to reduce the integration times by a factor of two to  $\lesssim 0.02$  s for Styx/Kerberos and by a factor of 2–3 to  $\lesssim 0.2$  s for Nix/Hydra.

### 3.3. Future Options

Although ground-based occultations and JWST IR imaging are the only current options for detecting smaller satellites in the Pluto–Charon system, we briefly consider whether planned missions are also capable of discovering new satellites.

WFIRST is a 2.4-m space telescope concept with a wide-field imager and a coronagraphic instrument (Green et al. 2012; Spergel et al. 2013). Despite having a sensitivity comparable with HST, the wide-field imager is not designed for the high contrast, high resolution observations required to detect existing or additional satellites in the Pluto–Charon system. The coronagraphic instrument is expected to achieve contrast ratios of  $10^{-9}$  or larger on scales of roughly  $1''$  (see also Burrows 2014; Lacy et al. 2018). Detecting very small satellites ( $r \ll 1$  km) and any faint debris in the system would be straightforward. The likely field-of-view has a radius of only  $2''$ ; thus, it would not be possible to center the coronagraph on Pluto and search for faint satellites beyond the orbit of Hydra. Still, it is worth exploring whether moving Pluto–Charon off the edge of the field would allow deep searches for faint satellites.

The Origins Space Telescope is a 6–9-m telescope concept with 4–5 proposed instruments (e.g., Meixner et al. 2017; Battersby et al. 2018). Designed to operate at wavelengths  $\lambda \gtrsim 5 \mu\text{m}$ , current plans do not include an imaging instrument similar to those on JWST or WFIRST. Unless designs change, this facility is unlikely to enable discovery of faint satellites in the Pluto–Charon system.

LUVOIR (ATLAST) is a 8–16-m ultraviolet–optical–infrared telescope concept with a variety of proposed instruments (e.g., Postman et al. 2009; Feinberg et al. 2014; Thronson et al. 2016; Bolcar et al. 2017; Arney et al. 2017). Scaling from quoted sensitivity estimates for instruments on the 6.5-m JWST, IR imagers on LUVOIR could detect small satellites beyond the orbit of Hydra with radii  $r \approx 0.5$ –1 km. Improvements in instrument efficiency would enable detection of smaller satellites. If the proposed coronagraph could reach a contrast of  $10^{-9}$  over a larger field-of-view, detection of m-sized objects might be possible.

The Habitable Exoplanet Observatory (HabEx) is a 4–8-m telescope concept designed to image exoplanets and to detect biosignatures in the spectra of exoplanets around nearby

stars (e.g., Mennesson et al. 2016). With an aperture comparable to JWST and wavelength coverage similar to LUVOIR, discovering satellites with  $r \lesssim 1$  km requires a coronagraph with new technology (e.g., Ruane et al. 2017, 2018). As with LUVOIR, reaching proposed contrasts of  $\sim 10^{-9}$  enables detection of much smaller satellites.

## 4. DISCUSSION

### 4.1. Dynamical Architecture of the Pluto–Charon Satellite System

The  $n$ -body calculations discussed here place new constraints on the dynamics of the Pluto–Charon satellite system. For the adopted masses of the four small satellites, the system is as tightly packed as possible. There are few stable orbits where satellites with negligible mass can exist between the orbit of Styx and the orbit of Hydra. This conclusion is independent of inclination angle: satellites on polar orbits are about as unstable as prograde satellites orbiting in the plane of the binary system.

There is also limited space for stable satellites on circumbinary orbits inside the orbit of Styx<sup>2</sup> (see also Holman & Wiegert 1999; Pichardo et al. 2008; Doolin & Blundell 2011; Youdin et al. 2012). From simulations without any small satellites, stable orbits could exist from 1.3–2.1  $a_{PC}$  (retrograde) and 1.7–2.1  $a_{PC}$  (prograde). Polar orbits inside the orbit of Styx are unstable. The new calculations yield a set of massless survivors on prograde orbits with initial semimajor axes  $a_0 \approx 1.8$ –2.1  $a_{PC}$ .

Well outside the orbit of Hydra, massless satellites on prograde and polar orbits are stable. With the nominal masses, Nix and Hydra clear out tracers with  $a \lesssim 1.08 a_H$  on time scales of 5–10 Myr. On longer time scales, orbits with  $a \approx 1.08 - 1.12 a_H$  are probably also unstable. Tracers with  $a \gtrsim 1.15 a_H$  appear to be stable.

Tests with massive satellites confirm these results. Although some massless tracers on prograde orbits survive for as long as 10 Myr near the corotation zones of Nix and Hydra, small satellites with  $r \approx 2$  km and  $m \approx 4 \times 10^{16}$  g on identical orbits have lifetimes as short as 10–1000 yr. Others survive for 100 Myr. Inside the orbit of Styx, small moons are ejected on time scales ranging from 1 yr to nearly 100 Myr. Small moons on polar orbits between Nix and Hydra are similarly unstable, with lifetimes ranging from  $10^3$  yr to 100 Myr. Given the loss rate in our calculations, it seems unlikely that additional satellites with  $r \gtrsim 2$  km

---

<sup>2</sup>For discussions of stability regions at smaller  $a$  (between Pluto and Charon), see Winter et al. (2010) and Giuliatti Winter et al. (2013, 2014, 2015).

inside the orbit of Hydra can survive for the age of the solar system.

Massive satellites outside the orbit of Hydra fare much better. After 150 Myr of evolution, roughly 90% of those on prograde orbits survive. Survivors tend to have larger initial semimajor axes than ejected moons. Small moons on polar orbits outside the orbit of Hydra are just as unlikely to be ejected after 100 Myr of evolution. Thus, searches for new satellites should concentrate on regions outside the orbit of Hydra.

Aside from clarifying our understanding of circumbinary dynamics, these results help to interpret the lack of new satellite detections from *New Horizons* imaging data. With additional satellites generally precluded at  $a \lesssim 1.1 a_H$ , the volume for discovering new, stable satellites within the overall *New Horizons* footprint  $a \lesssim 1.6 a_H$  is restricted. While it is not surprising that *New Horizons* failed to detect new satellites inside the orbit of Hydra, the lack of 2–3 km satellites outside the orbit of Hydra is surprising. Perhaps they never formed or were ejected. If smaller than the *New Horizons* threshold of 2 km, they await detection with a new generation of instruments.

The calculations of massless tracers orbiting between Styx and Hydra also provide new insights into the lack of emission from small particles detected from *New Horizons* data (Lauer et al. 2018). Prior to the *New Horizons* flyby, several studies derived upper limits on small moons and dust emission from direct imaging (e.g., Steffl et al. 2006; Marton et al. 2015) and occultations (Boissel et al. 2014; Throop et al. 2015). Theoretical studies based on  $n$ -body simulations predicted steady-state optical depths from a balance between dust production from impacts on Pluto–Charon and the smaller satellites and losses from radiation pressure and dynamical ejections (Stern et al. 2006; Pires Dos Santos et al. 2011; Poppe & Horányi 2011; Pires dos Santos et al. 2013). The new results described here demonstrate that all orbits from  $1.7 a_{PC}$  to  $3.6$ – $3.7 a_{PC}$  are dynamically unstable on time scales ranging from several decades to 10 Myr. Without additional dust production from impacts, our results imply that there should be no dust or larger particles inside the orbit of Hydra.

If small particles or dust emission are ever detected in the Pluto–Charon system, the mass and location of small particles place interesting constraints on the masses of the four small satellites. If limits on the production rate for small particles from impacts can be established from *New Horizons* data, the number of survivors between the orbits of Styx and Hydra is sensitive to the mass of Nix and Hydra: smaller masses for these satellites allow larger masses in dust (see also Stern et al. 2006; Pires Dos Santos et al. 2011; Poppe & Horányi 2011; Pires dos Santos et al. 2013).

Identifying new satellites or small particles outside the orbit of Hydra would also improve estimates for the mass of Hydra. From the  $n$ -body calculations, the innermost stable orbit

outside Hydra is much more sensitive to Hydra’s mass than to the mass of Nix or the other satellites (see also Michaely et al. 2017). Accurate measurements of the orbital elements for any new satellite would thus provide new limits on Hydra’s mass.

## 4.2. JWST Feasibility

Although the current launch date for JWST is not until 2021 March, the observations proposed here are similar to the suite of HST imaging data collected prior to the *New Horizons* flyby (e.g., Weaver et al. 2006; Buie et al. 2006; Steffl et al. 2006; Steffl & Stern 2007; Tholen et al. 2008; Showalter et al. 2011, 2012; Brozović et al. 2015; Showalter & Hamilton 2015). Starting in Cycle 2, various HST imaging programs sought to constrain the properties of dusty structures and satellites in the Pluto–Charon system. These programs acquired many images per HST orbit, with exposure times ranging from a few seconds to several minutes. As outlined in Brozović et al. (2015), multiple images per orbit enable a robust analysis procedure which eliminates light from background stars and provides the best possible signal-to-noise for images of very faint satellites.

We anticipate that a JWST observing program to detect faint satellites in the Pluto–Charon system would be similar to a typical Hubble program. Within a single visit, the likely total exposure time with JWST imagers would probably be several times longer than an HST orbit. As outlined in Gordon et al. (2015) for MIRI, multiple short and moderate exposures would allow the same type of analysis procedure as performed by Brozović et al. (2015).

Aside from the ability of JWST instruments to perform to specifications, the main uncertainty in any JWST program is the overhead involved in acquiring a target, maintaining a fix on the target, conducting the observations, and performing the housekeeping needed for the health of the satellite. Various performance analyses suggest the typical overhead in an observing program is roughly 30% (Gordon et al. 2012a,b). Thus, the program outlined here seems feasible.

## 4.3. Occultation Feasibility

Over the past few decades, various groups have observed Pluto and Charon occult fairly bright stars to infer the extent and physical properties of their atmospheres and to plan for the *New Horizons* flyby (e.g., Person et al. 2006; Sicardy et al. 2011; Person et al. 2013; Throop et al. 2015; Gulbis et al. 2015; Bosh et al. 2015; Dias-Oliveira et al. 2015; Sicardy

et al. 2016; Pasachoff et al. 2016, 2017, and references therein). With exposure times of 0.25 to 5 sec on 1-m to 2.5-m telescopes, the typical signal-to-noise ranges from roughly 10 to better than 100.

Detailed astrometric analyses demonstrate that occultations by the Pluto–Charon system are fairly frequent. For 2008–2015, predictions by Assafin et al. (2010) indicate 30–300 possible occultations per year for each of Pluto, Charon, Nix, and Hydra. Although we are unaware of similar published predictions for Styx and Kerberos, it seems likely from Assafin et al. (2010) that the frequency of occultations for both of these small moons is similar to that for Nix and Hydra. The uncertain orbital path of Pluto across the sky is the main limitation in these predictions (e.g., Benedetti-Rossi et al. 2014; Holman & Payne 2016, and references therein).

Many studies have explored the possibility of using occultations to detect small Kuiper belt objects beyond 40–50 AU (KBOs; e.g., Bailey 1976; Brown & Webster 1997; Alcock et al. 2003; Cooray & Farmer 2003; Cooray 2003; Chang et al. 2006; Roques et al. 2006; Bickerton et al. 2008; Bianco et al. 2009; Schlichting et al. 2009; Wang et al. 2009; Bianco et al. 2010; Wang et al. 2010; Chang et al. 2011; Schlichting et al. 2012; Zhang et al. 2013, and references therein). Aside from ground-based optical observations, HST and RXTE have yielded promising sets of data to search for serendipitous occultations of stellar sources by KBOs. On the ground and with HST, exposure times of 0.02 sec yield light curves with sufficient signal-to-noise to detect KBOs with radii of roughly 1 km.

Based on this discussion, it seems straightforward to detect occultations of stars by Pluto’s known small satellites with modest aperture ground-based telescopes. However, the likelihood of detecting a serendipitous occultation event from an unknown satellite is small. Assuming a satellite with a diameter  $D_6 \approx 2$  km is positioned randomly in an orbit with semimajor axis  $a_6 \approx 75,000$  km (outside Hydra), the chance of having it along the same occultation path as any of the other small satellites is less than  $2D_6/2\pi a_6 \lesssim 10^{-5}$ . With  $N$  of these satellites, the probability is still small,  $10^{-5}N$ , unless  $N$  is very large.

Overall, the best strategy to detect and to characterize new satellites involves initial imaging observations with JWST followed by ground-based occultation observations. Although JWST data are fairly expensive and limited by spacecraft constraints, observations with any of the imaging instruments sample broad swaths of available discovery space. If new satellites are detected, occultations can then provide additional information on the orbits and shapes.

#### 4.4. Connections with Exo-Planetary Systems

Over the past few decades, various techniques have revealed  $\sim 15$  circumbinary planetary systems (Thorsett et al. 1993; Doyle et al. 2011; Welsh et al. 2012; Orosz et al. 2012a,b; Schwamb et al. 2013; Kostov et al. 2013; Bailey et al. 2014; Kostov et al. 2014, 2016; Jain et al. 2017; Getley et al. 2017). Aside from systems with main sequence stars, the binaries include a binary pulsar and a low mass X-ray binary. Planet masses range from  $\sim$  Neptune up to  $\sim$  seven times Jupiter. Often, the circumbinary planets orbit in the plane of the inner binary and are reasonably close to the innermost stable orbit. In several, the orbit of the planet is somewhat tilted with respect to the inner binary. Sometimes, the planet is well outside the innermost orbit.

The formation and evolution of circumbinary planets have attracted intense theoretical interest (e.g., Pierens & Nelson 2007, 2008a,b; Paardekooper et al. 2012; Rafikov 2013; Pierens & Nelson 2013; Rafikov & Silsbee 2015a,b; Silsbee & Rafikov 2015b,a; Bromley & Kenyon 2015a; Kley & Haghighipour 2015; Vartanyan et al. 2016; Hamers et al. 2016; Li et al. 2016; Mutter et al. 2017a,b; Quarles et al. 2018; Fleming et al. 2018; Pierens & Nelson 2018; Zanazzi & Lai 2018; Thun & Kley 2018, and references therein). In addition to changing the structure and evolution of a planet-forming gaseous disk, the central binary provides a challenging environment for the growth of Earth-mass and larger planets from km-sized and larger planetesimals. Once planets form, the central binary efficiently removes them from resonant orbits. Multi-planet systems are particularly prone to disruption.

Although there are currently no circumbinary planetary systems with more than one planet, there are numerous multi-planet systems orbiting single stars (e.g., Lissauer et al. 2011, 2012; Rowe et al. 2014; Fabrycky et al. 2014; Lissauer et al. 2014; Winn & Fabrycky 2015; Ballard & Johnson 2016; Sinukoff et al. 2016; Udry et al. 2017; Weiss et al. 2018, and references therein). Many of these are closely-packed, with little or no space for additional planets between the innermost and outermost planets. In each multi-planet system, the planets are often of similar size, with the outermost planet usually the largest (see also Ciardi et al. 2013; Millholland et al. 2017). Sometimes, the planets have very different sizes.

Theoretical studies of closely-packed multi-planet systems focus on their origin and stability (e.g. Rein 2012; Hansen & Murray 2012, 2013; Raymond & Cossou 2014; Schlaufman 2014; Najita & Kenyon 2014; Steffen & Hwang 2015; Malhotra 2015; Pu & Wu 2015; Batygin & Laughlin 2015; Morrison & Kratter 2016; Pan & Schlichting 2017; Mustill et al. 2017, and references therein). Formation at several AU distances followed by migration through a circumstellar gaseous disk is a favored explanation for many close-in multi-planet systems. However, *in situ* growth is also a possibility. In both mechanisms, it is unclear how the most closely-packed planetary systems form and maintain their stability on Gyr time scales.

Together with previous theoretical studies of the Pluto–Charon system (Canup 2005; Ward & Canup 2006; Lee & Peale 2006; Lithwick & Wu 2008b,a; Canup 2011; Youdin et al. 2012; Kenyon & Bromley 2014b; Cheng et al. 2014; Desch 2015; Pires et al. 2015; Walsh & Levison 2015; Bromley & Kenyon 2015b; Michaely et al. 2017; Smullen & Kratter 2017; McKinnon et al. 2017; Woo & Lee 2018), the results described here inform our understanding of circumbinary planets and closely-packed planetary systems orbiting single or binary stars. Despite forming in a relatively gas-free environment, the Pluto–Charon system has issues with *in situ* formation, migration, orbital resonances, and long-term stability similar to those in exoplanetary systems. Nevertheless, the small satellites probably (i) grew from a ring of debris, (ii) found stable orbits close to resonances with the central binary, and (iii) maintained these orbits for  $\sim 4$  Gyr (Weaver et al. 2016; Robbins et al. 2017). Working out the details of this history for the Pluto–Charon satellites and exoplanetary systems will enrich theories of planet formation.

## 5. SUMMARY

We have analyzed a large suite of  $n$ -body calculations to isolate stable orbits for additional satellites in the Pluto–Charon system. Although there are few stable low inclination, prograde orbits or high inclination, polar orbits for massless tracers with semimajor axes,  $0.9 a_S \lesssim a \lesssim 1.1 a_H$ , low eccentricity orbits with  $a \gtrsim 1.1 a_H$  are stable. Within this range of semimajor axes, polar and prograde orbits are equally stable.

Tests with massive satellites ( $r \approx 2$  km) confirm the stability of orbits well beyond the orbit of Hydra. Among an ensemble of satellites with  $a_0 \approx 3.7\text{--}4.0 a_{PC}$ , nearly all survive 100–150 Myr of dynamical evolution. Calculations of satellites with smaller  $a_0$  have many fewer survivors after 100–150 Myr. Thus, the best region to search for new satellites in the Pluto–Charon system is beyond the orbit of Hydra.

Several types of observations could detect small satellites on these orbits. Direct imaging with JWST can reveal 1–2 km satellites with modest integration times. Although discovering such small satellites with stellar occultations is a challenge, observations with 2–3-m class telescopes can detect the signal from the occultation of a nearby solar-type star by a 1–2 km satellite. In the (far) future, observations with WFIRST or ATLAST may reveal even smaller satellites and a debris disk or ring(s).

Finding additional small satellites in the Pluto–Charon system constrains the masses of the known satellites and provides additional tests of theoretical models for satellite formation. Discovery of small objects between the orbits of Styx and Hydra would require lower mass

(and mass density) for Nix and Hydra. Any satellite orbiting beyond Hydra might reduce the uncertainty in the mass of Hydra. Current theory predicts several satellites with  $r \approx 1\text{--}3$  km and  $a \approx 1.5\text{--}2.5 a_H$ . Observations with JWST and ground-based telescopes can test this theory and improve our understanding of circumbinary satellite formation.

Resources supporting this work on the ‘discover’ cluster were provided by the NASA High-End Computing (HEC) Program through the NASA Center for Climate Simulation (NCCS) at Goddard Space Flight Center. Advice and comments from T. Currie, M. Geller, M. Payne, and A. Youdin greatly improved our presentation. Portions of this project were supported by the *NASA Outer Planets* and *Emerging Worlds* programs through grants NNX11AM37G and NNX17AE24G.

### A. Tests of the Symplectic Integrator

To track the orbital evolution of the Pluto–Charon system, our  $n$ -body code employs an adaptive sixth-order accurate algorithm based on either Richardson extrapolation (Bromley & Kenyon 2006) or a symplectic method (Yoshida 1990; Wisdom & Holman 1991; Saha & Tremaine 1992). The code calculates gravitational forces by direct summation and evolves particles in the center-of-mass frame. Aside from passing a stringent set of dynamical tests and benchmarks (Duncan et al. 1998; Bromley & Kenyon 2006), we have used the code to simulate scattering of super-Earths by growing gas giants (Bromley & Kenyon 2011a), migration through planetesimal disks (Bromley & Kenyon 2011b) and Saturn’s rings (Bromley & Kenyon 2013), the formation of Pluto’s small satellites (Kenyon & Bromley 2014a), and the circularization of the orbits of planet scattered into the outer solar system (Bromley & Kenyon 2014, 2016).

To evolve the orbit of the Pluto–Charon satellites in time, the time step in our symplectic algorithm is  $\Delta t = T_{PC}/N$  where  $T_{PC}$  is the orbital period of the central binary and  $N$  is an integer. For any simulation, the total cpu time is proportional to  $N$ . To select a value for  $N$  which maintains the integrity of the solution in a reasonable amount of cpu time, we consider the orbit of an idealized Pluto–Charon binary with the measured masses and orbital semimajor axes and orbital eccentricity  $10^{-4}$ ,  $10^{-5}$ ,  $10^{-6}$ , and  $10^{-7}$ . For  $N = 20\text{--}150$ , we evolve the binary orbit for 100 Myr and record the position  $(x, y, z)$  and velocity  $(\dot{x}, \dot{y}, \dot{z})$  vectors and the osculating orbital elements  $a$  and  $e$  every 10–100 binary orbits. To evaluate the ability of the code to track  $a$  and  $e$ , we derive the average, standard deviation, median, and inter-quartile range over  $M$  time steps. Typically, the median is indistinguishable from

the average; the inter-quartile range is nearly identical to the standard deviation. Using standard estimates for the linear correlation coefficient (Pearson’s  $r$ ), the Spearman rank-order correlation coefficient, and Kendall’s  $\tau$  (Press et al. 1992), we look for trends in  $a$ ,  $e$ , and  $i$  with evolution time.

In these tests, there is no indication that the average/median  $a$  (and its standard deviation or inter-quartile range) or any trend in  $a$  and  $e$  with time depend on the number of steps per binary orbit. For the semimajor axis, the vanishingly small dispersion and inter-quartile range are independent of  $M$ . Typical correlation coefficients of  $a$  and  $e$  with time are  $\pm 10^{-3}$  or smaller. Thus, none of our calculations experience any drift in  $a$  or  $e$  over 100 Myr of evolution.

Trends of the average  $e$  and the standard deviation in  $e$  with  $N$  are very clear (12). For the  $e = 10^{-7}$  binary (orange symbols), calculations with  $N \geq 100$  reliably maintain the initial orbital configuration. Results for  $N = 20$ – $30$  are especially poor. When  $e = 10^{-6}$  (green symbols), calculations with  $N \geq 70$  sustain the initial  $e$ . Faithfully tracking the orbits of binaries with larger  $e$  requires fewer steps per binary orbit,  $N = 30$  for  $e = 10^{-4}$  (purple symbols) and  $N \approx 40$ – $50$  for  $e = 10^{-5}$  (blue symbols). With a measured  $e \approx 5 \times 10^{-5}$  (as indicated by the horizontal grey line), calculations with  $N = 40$  preserve the measured  $e$  of Pluto–Charon.

Long (100–500 Myr) simulations of Pluto–Charon and the four satellites yield similar results for trends in  $a(t)$  and  $e(t)$  of the central binary. As long as the satellite system remains stable, there is no trend in  $a$  or  $e$  of the Pluto–Charon binary or the small satellites. We plan to describe the results of these simulations in a separate publication.

## REFERENCES

- Alcock, C., Dave, R., Giammarco, J., et al. 2003, *Earth Moon and Planets*, 92, 459
- Arney, G. N., Crooke, J., Domagal-Goldman, S. D., et al. 2017, *AGU Fall Meeting Abstracts*
- Assafin, M., Camargo, J. I. B., Vieira Martins, R., et al. 2010, *A&A*, 515, A32
- Bagenal, F., Horányi, M., McComas, D. J., et al. 2016, *Science*, 351, aad9045
- Bailey, M. E. 1976, *Nature*, 259, 290
- Bailey, V., Meshkat, T., Reiter, M., et al. 2014, *ApJ*, 780, L4
- Ballard, S., & Johnson, J. A. 2016, *ApJ*, 816, 66

- Battersby, C., Armus, L., Bergin, E., et al. 2018, *Nature Astronomy*, 2, 596
- Batygin, K., & Laughlin, G. 2015, *Proceedings of the National Academy of Science*, 112, 4214
- Beichman, C. A., Rieke, M., Eisenstein, D., et al. 2012, in *Proc. SPIE, Vol. 8442, Space Telescopes and Instrumentation 2012: Optical, Infrared, and Millimeter Wave*, 84422N
- Benedetti-Rossi, G., Vieira Martins, R., Camargo, J. I. B., Assafin, M., & Braga-Ribas, F. 2014, *A&A*, 570, A86
- Bianco, F. B., Protopapas, P., McLeod, B. A., et al. 2009, *AJ*, 138, 568
- Bianco, F. B., Zhang, Z.-W., Lehner, M. J., et al. 2010, *AJ*, 139, 1499
- Bickerton, S. J., Kavelaars, J. J., & Welch, D. L. 2008, *AJ*, 135, 1039
- Boissel, Y., Sicardy, B., Roques, F., et al. 2014, *A&A*, 561, A144
- Bolcar, M. R., Alosez, S., Bly, V. T., et al. 2017, in *Society of Photo-Optical Instrumentation Engineers (SPIE) Conference Series, Vol. 10398, Society of Photo-Optical Instrumentation Engineers (SPIE) Conference Series*, 1039809
- Bosh, A. S., Person, M. J., Levine, S. E., et al. 2015, *Icarus*, 246, 237
- Bromley, B. C., & Kenyon, S. J. 2006, *AJ*, 131, 2737
- . 2011a, *ApJ*, 731, 101
- . 2011b, *ApJ*, 735, 29
- . 2013, *ApJ*, 764, 192
- . 2014, *ApJ*, 796, 141
- . 2015a, *ApJ*, 806, 98
- . 2015b, *ApJ*, 809, 88
- . 2016, *ApJ*, 826, 64
- . 2017, *AJ*, 153, 216
- Brown, M. J. I., & Webster, R. L. 1997, *MNRAS*, 289, 783
- Brozović, M., Showalter, M. R., Jacobson, R. A., & Buie, M. W. 2015, *Icarus*, 246, 317

- Buie, M. W., Grundy, W. M., & Tholen, D. J. 2013, *AJ*, 146, 152
- Buie, M. W., Grundy, W. M., Young, E. F., Young, L. A., & Stern, S. A. 2006, *AJ*, 132, 290
- Buie, M. W., Tholen, D. J., & Grundy, W. M. 2012, *AJ*, 144, 15
- Burrows, A. 2014, ArXiv e-prints, arXiv:1412.6097
- Canup, R. M. 2005, *Science*, 307, 546
- . 2011, *AJ*, 141, 35
- Chambers, J. E., Wetherill, G. W., & Boss, A. P. 1996, *Icarus*, 119, 261
- Chang, H.-K., King, S.-K., Liang, J.-S., et al. 2006, *Nature*, 442, 660
- Chang, H.-K., Liu, C.-Y., & Chen, K.-T. 2011, *MNRAS*, 411, 427
- Cheng, W. H., Peale, S. J., & Lee, M. H. 2014, *Icarus*, 241, 180
- Ciardi, D. R., Fabrycky, D. C., Ford, E. B., et al. 2013, *ApJ*, 763, 41
- Cook, J. C., Ore, C. M. D., Protopapa, S., et al. 2018, *Icarus*, 315, 30
- Cooray, A. 2003, *ApJ*, 589, L97
- Cooray, A., & Farmer, A. J. 2003, *ApJ*, 587, L125
- Deck, K. M., Payne, M., & Holman, M. J. 2013, *ApJ*, 774, 129
- Desch, S. J. 2015, *Icarus*, 246, 37
- Dias-Oliveira, A., Sicardy, B., Lellouch, E., et al. 2015, *ApJ*, 811, 53
- Doolin, S., & Blundell, K. M. 2011, *MNRAS*, 418, 2656
- Doyle, L. R., Carter, J. A., Fabrycky, D. C., et al. 2011, *Science*, 333, 1602
- Doyon, R., Hutchings, J. B., Beaulieu, M., et al. 2012, in *Proc. SPIE*, Vol. 8442, *Space Telescopes and Instrumentation 2012: Optical, Infrared, and Millimeter Wave*, 84422R
- Duncan, M. J., & Levison, H. F. 1997, *Science*, 276, 1670
- Duncan, M. J., Levison, H. F., & Lee, M. H. 1998, *AJ*, 116, 2067
- Dvorak, R., Froeschle, C., & Froeschle, C. 1989, *A&A*, 226, 335

- Elliot, J. L., Dunham, E. W., Bosh, A. S., et al. 1989, *Icarus*, 77, 148
- Elliot, J. L., Person, M. J., & Qu, S. 2003, *AJ*, 126, 1041
- Fabrycky, D. C., Lissauer, J. J., Ragozzine, D., et al. 2014, *ApJ*, 790, 146
- Fang, J., & Margot, J.-L. 2013, *ApJ*, 767, 115
- Farago, F., & Laskar, J. 2010, *MNRAS*, 401, 1189
- Feinberg, L. D., Jones, A., Mosier, G., et al. 2014, in *Proc. SPIE*, Vol. 9143, *Space Telescopes and Instrumentation 2014: Optical, Infrared, and Millimeter Wave*, 914316
- Fleming, D. P., Barnes, R., Graham, D. E., Luger, R., & Quinn, T. R. 2018, *ApJ*, 858, 86
- Getley, A. K., Carter, B., King, R., & O’Toole, S. 2017, *MNRAS*, 468, 2932
- Giuliatti Winter, S. M., Winter, O. C., Vieira Neto, E., & Sfair, R. 2013, *MNRAS*, 430, 1892
- . 2014, *MNRAS*, 439, 3300
- . 2015, *Icarus*, 246, 339
- Gladman, B. 1993, *Icarus*, 106, 247
- Gladman, B., Holman, M., Grav, T., et al. 2002, *Icarus*, 157, 269
- Gordon, K. D., Kinzel, W., Balzano, V., et al. 2012a, *JWST-StSCI*, 002564, 002564
- Gordon, K. D., Balzano, V., Blair, W., et al. 2012b, in *Proc. SPIE*, Vol. 8448, *Observatory Operations: Strategies, Processes, and Systems IV*, 84481U
- Gordon, K. D., Chen, C. H., Anderson, R. E., et al. 2015, *PASP*, 127, 696
- Green, J., Schechter, P., Baltay, C., et al. 2012, *ArXiv e-prints*, arXiv:1208.4012
- Grundy, W. M., Binzel, R. P., Buratti, B. J., et al. 2016, *Science*, 351, aad9189
- Gulbis, A. A. S., Emery, J. P., Person, M. J., et al. 2015, *Icarus*, 246, 226
- Hamers, A. S., Perets, H. B., & Portegies Zwart, S. F. 2016, *MNRAS*, 455, 3180
- Hansen, B. M. S., & Murray, N. 2012, *ApJ*, 751, 158
- . 2013, *ApJ*, 775, 53
- Holman, M. J., & Payne, M. J. 2016, *AJ*, 152, 80

- Holman, M. J., & Wiegert, P. A. 1999, *AJ*, 117, 621
- Hubbard, W. B., Hunten, D. M., Dieters, S. W., Hill, K. M., & Watson, R. D. 1988, *Nature*, 336, 452
- Jain, C., Paul, B., Sharma, R., Jaleel, A., & Dutta, A. 2017, *MNRAS*, 468, L118
- Kenyon, S. J. 2002, *PASP*, 114, 265
- Kenyon, S. J., & Bromley, B. C. 2008, *ApJS*, 179, 451
- . 2014a, *ApJ*, 780, 4
- . 2014b, *AJ*, 147, 8
- . 2016, *ApJ*, 817, 51
- Kenyon, S. J., Najita, J. R., & Bromley, B. C. 2016, *ApJ*, 831, 8
- Kley, W., & Haghighipour, N. 2015, *A&A*, 581, A20
- Kostov, V. B., McCullough, P. R., Hinse, T. C., et al. 2013, *ApJ*, 770, 52
- Kostov, V. B., McCullough, P. R., Carter, J. A., et al. 2014, *ApJ*, 784, 14
- Kostov, V. B., Orosz, J. A., Welsh, W. F., et al. 2016, *ApJ*, 827, 86
- Lacy, B., Shlivko, D., & Burrows, A. 2018, *ArXiv e-prints*, arXiv:1801.08964
- Lauer, T. R., Throop, H. B., Showalter, M. R., et al. 2018, *Icarus*, 301, 155
- Lee, M. H., & Peale, S. J. 2006, *Icarus*, 184, 573
- Leung, G. C. K., & Lee, M. H. 2013, *ApJ*, 763, 107
- Li, G., Holman, M. J., & Tao, M. 2016, *ApJ*, 831, 96
- Lissauer, J. J., Ragozzine, D., Fabrycky, D. C., et al. 2011, *ApJS*, 197, 8
- Lissauer, J. J., Marcy, G. W., Rowe, J. F., et al. 2012, *ApJ*, 750, 112
- Lissauer, J. J., Marcy, G. W., Bryson, S. T., et al. 2014, *ApJ*, 784, 44
- Lithwick, Y., & Wu, Y. 2008a, *ArXiv e-prints*, arXiv:0802.2951
- . 2008b, *ArXiv e-prints*, arXiv:0802.2939

- Mahajan, N., & Wu, Y. 2014, *ApJ*, 795, 32
- Malhotra, R. 2015, *ApJ*, 808, 71
- Marton, G., Kiss, C., Balog, Z., et al. 2015, *A&A*, 579, L9
- McKinnon, W. B., Stern, S. A., Weaver, H. A., et al. 2017, *Icarus*, 287, 2
- Meixner, M., Cooray, A., Leisawitz, D., Staguhn, J., & Origins Space Telescope STDT. 2017, in *LPI Contributions*, Vol. 2042, *Habitable Worlds 2017: A System Science Workshop*, 4152
- Mennesson, B., Gaudi, S., Seager, S., et al. 2016, in *Proc. SPIE*, Vol. 9904, *Space Telescopes and Instrumentation 2016: Optical, Infrared, and Millimeter Wave*, 99040L
- Michaely, E., Perets, H. B., & Grishin, E. 2017, *ApJ*, 836, 27
- Millholland, S., Wang, S., & Laughlin, G. 2017, *ApJ*, 849, L33
- Morrison, S. J., & Kratter, K. M. 2016, *ApJ*, 823, 118
- Musielak, Z. E., Cuntz, M., Marshall, E. A., & Stuit, T. D. 2005, *A&A*, 434, 355
- Mustill, A. J., Davies, M. B., & Johansen, A. 2017, *MNRAS*, 468, 3000
- Mutter, M. M., Pierens, A., & Nelson, R. P. 2017a, *MNRAS*, 465, 4735
- . 2017b, *MNRAS*, 469, 4504
- Najita, J. R., & Kenyon, S. J. 2014, *MNRAS*, 445, 3315
- Nihei, T. C., Lehner, M. J., Bianco, F. B., et al. 2007, *AJ*, 134, 1596
- Nimmo, F., Umurhan, O., Lisse, C. M., et al. 2017, *Icarus*, 287, 12
- Obertas, A., Van Laerhoven, C., & Tamayo, D. 2017, *Icarus*, 293, 52
- Orosz, J. A., Welsh, W. F., Carter, J. A., et al. 2012a, *Science*, 337, 1511
- . 2012b, *ApJ*, 758, 87
- Paardekooper, S.-J., Leinhardt, Z. M., Thébault, P., & Baruteau, C. 2012, *ApJ*, 754, L16
- Pan, M., & Schlichting, H. E. 2017, *ArXiv e-prints*, arXiv:1704.07836
- Pasachoff, J. M., Souza, S. P., Babcock, B. A., et al. 2005, *AJ*, 129, 1718

- Pasachoff, J. M., Person, M. J., Bosh, A. S., et al. 2016, *AJ*, 151, 97
- Pasachoff, J. M., Babcock, B. A., Durst, R. F., et al. 2017, *Icarus*, 296, 305
- Person, M. J., Elliot, J. L., Gulbis, A. A. S., et al. 2006, *AJ*, 132, 1575
- Person, M. J., Dunham, E. W., Bosh, A. S., et al. 2013, *AJ*, 146, 83
- Petit, J., & Henon, M. 1986, *Icarus*, 66, 536
- Pichardo, B., Sparke, L. S., & Aguilar, L. A. 2005, *MNRAS*, 359, 521
- . 2008, *MNRAS*, 391, 815
- Pierens, A., & Nelson, R. P. 2007, *A&A*, 472, 993
- . 2008a, *A&A*, 478, 939
- . 2008b, *A&A*, 483, 633
- . 2013, *A&A*, 556, A134
- . 2018, *MNRAS*, 477, 2547
- Pilat-Lohinger, E., Funk, B., & Dvorak, R. 2003, *A&A*, 400, 1085
- Pires, P., Giuliatti Winter, S. M., & Gomes, R. S. 2015, *Icarus*, 246, 330
- Pires Dos Santos, P. M., Giuliatti Winter, S. M., & Sfair, R. 2011, *MNRAS*, 410, 273
- Pires dos Santos, P. M., Giuliatti Winter, S. M., Sfair, R., & Mourão, D. C. 2013, *MNRAS*, 430, 2761
- Poppe, A., & Horányi, M. 2011, *Planet. Space Sci.*, 59, 1647
- Porter, S. B., & Stern, S. A. 2015, *ArXiv e-prints*, arXiv:1505.05933
- Postman, M., Argabright, V., Arnold, B., et al. 2009, *ArXiv e-prints*, arXiv:0904.0941
- Press, W. H., Teukolsky, S. A., Vetterling, W. T., & Flannery, B. P. 1992, *Numerical recipes in FORTRAN. The art of scientific computing* (Cambridge: University Press)
- Pu, B., & Wu, Y. 2015, *ApJ*, 807, 44
- Quarles, B., Satyal, S., Kostov, V., Kaib, N., & Haghhighipour, N. 2018, *ApJ*, 856, 150
- Rafikov, R. R. 2013, *ApJ*, 764, L16

- Rafikov, R. R., & Silsbee, K. 2015a, *ApJ*, 798, 69
- . 2015b, *ApJ*, 798, 70
- Raymond, S. N., & Cossou, C. 2014, *MNRAS*, 440, L11
- Rein, H. 2012, *MNRAS*, 427, L21
- Rieke, G. H., Wright, G. S., Böker, T., et al. 2015, *PASP*, 127, 584
- Robbins, S. J., Singer, K. N., Bray, V. J., et al. 2017, *Icarus*, 287, 187
- Roques, F., Doressoundiram, A., Dhillon, V., et al. 2006, *AJ*, 132, 819
- Rowe, J. F., Bryson, S. T., Marcy, G. W., et al. 2014, *ApJ*, 784, 45
- Ruane, G., Mawet, D., Jewell, J., & Shaklan, S. 2017, in *Society of Photo-Optical Instrumentation Engineers (SPIE) Conference Series*, Vol. 10400, *Society of Photo-Optical Instrumentation Engineers (SPIE) Conference Series*, 104000J
- Ruane, G., Mawet, D., Mennesson, B., Jewell, J., & Shaklan, S. 2018, *Journal of Astronomical Telescopes, Instruments, and Systems*, 4, 015004
- Saha, P., & Tremaine, S. 1992, *AJ*, 104, 1633
- Schlaufman, K. C. 2014, *ApJ*, 790, 91
- Schlichting, H. E., Ofek, E. O., Wenz, M., et al. 2009, *Nature*, 462, 895
- Schlichting, H. E., Ofek, E. O., Sari, R., et al. 2012, *ApJ*, 761, 150
- Schwamb, M. E., Orosz, J. A., Carter, J. A., et al. 2013, *ApJ*, 768, 127
- Showalter, M. R., & Hamilton, D. P. 2015, *Nature*, 522, 45
- Showalter, M. R., Hamilton, D. P., Stern, S. A., et al. 2011, *IAU Circ.*, 9221, 1
- Showalter, M. R., Weaver, H. A., Stern, S. A., et al. 2012, *IAU Circ.*, 9253, 1
- Sicardy, B., Bolt, G., Broughton, J., et al. 2011, *AJ*, 141, 67
- Sicardy, B., Talbot, J., Meza, E., et al. 2016, *ApJ*, 819, L38
- Silsbee, K., & Rafikov, R. R. 2015a, *ArXiv e-prints*, arXiv:1504.00460
- . 2015b, *ApJ*, 798, 71

- Sinukoff, E., Howard, A. W., Petigura, E. A., et al. 2016, *ApJ*, 827, 78
- Smullen, R. A., & Kratter, K. M. 2017, *MNRAS*, 466, 4480
- Spergel, D., Gehrels, N., Breckinridge, J., et al. 2013, *ArXiv e-prints*, arXiv:1305.5422
- Steffen, J. H., & Hwang, J. A. 2015, *MNRAS*, 448, 1956
- Steffl, A. J., & Stern, S. A. 2007, *AJ*, 133, 1485
- Steffl, A. J., Mutchler, M. J., Weaver, H. A., et al. 2006, *AJ*, 132, 614
- Stern, S. A., Weaver, H. A., Steffl, A. J., et al. 2006, *Nature*, 439, 946
- Stern, S. A., Bagenal, F., Ennico, K., et al. 2015, *Science*, 350, aad1815
- Tholen, D. J., Buie, M. W., Grundy, W. M., & Elliott, G. T. 2008, *AJ*, 135, 777
- Thorsett, S. E., Arzoumanian, Z., & Taylor, J. H. 1993, *ApJ*, 412, L33
- Thronson, H., Bolcar, M. R., Clampin, M., et al. 2016, *Journal of Astronomical Telescopes, Instruments, and Systems*, 2, 041210
- Throop, H. B., French, R. G., Shoemaker, K., et al. 2015, *Icarus*, 246, 345
- Thun, D., & Kley, W. 2018, *A&A*, 616, A47
- Udry, S., Dumusque, X., Lovis, C., et al. 2017, *ArXiv e-prints*, arXiv:1705.05153
- Vartanyan, D., Garmilla, J. A., & Rafikov, R. R. 2016, *ApJ*, 816, 94
- Verbiscer, A. J., Porter, S. B., Buratti, B. J., et al. 2018, *ApJ*, 852, L35
- Verrier, P. E., & Evans, N. W. 2009, *MNRAS*, 394, 1721
- Walsh, K. J., & Levison, H. F. 2015, *ArXiv e-prints*, arXiv:1505.01208
- Wang, J.-H., Lehner, M. J., Zhang, Z.-W., et al. 2009, *AJ*, 138, 1893
- Wang, J.-H., Protopapas, P., Chen, W.-P., et al. 2010, *AJ*, 139, 2003
- Ward, W. R., & Canup, R. M. 2006, *Science*, 313, 1107
- Weaver, H. A., Stern, S. A., Mutchler, M. J., et al. 2006, *Nature*, 439, 943
- Weaver, H. A., Buie, M. W., Buratti, B. J., et al. 2016, *Science*, 351, aae0030

- Weiss, L. M., Marcy, G. W., Petigura, E. A., et al. 2018, *AJ*, 155, 48
- Welsh, W. F., Orosz, J. A., Carter, J. A., et al. 2012, *Nature*, 481, 475
- Wiegert, P. A., & Holman, M. J. 1997, *AJ*, 113, 1445
- Winn, J. N., & Fabrycky, D. C. 2015, *ARA&A*, 53, 409
- Winter, S. M. G., Winter, O. C., Guimarães, A. H. F., & Silva, M. R. 2010, *MNRAS*, 404, 442
- Wisdom, J. 1980, *AJ*, 85, 1122
- Wisdom, J., & Holman, M. 1991, *AJ*, 102, 1528
- Woo, J. M. Y., & Lee, M. H. 2018, *AJ*, 155, 175
- Yoshida, H. 1990, *Physics Letters A*, 150, 262
- Youdin, A. N., Kratter, K. M., & Kenyon, S. J. 2012, *ApJ*, 755, 17
- Young, E. F., & Binzel, R. P. 1994, *Icarus*, 108, 219
- Zanazzi, J. J., & Lai, D. 2018, *MNRAS*, 478, 835
- Zhang, Z.-W., Lehner, M. J., Wang, J.-H., et al. 2013, *AJ*, 146, 14

Table 1. Nominal satellite properties for  $n$ -body calculations<sup>a</sup>

Satellite	$m_s$	$r_s$ (km)	$\rho_s$	$r_H$ (km)	$a$ (km)	$a/a_{PC}$	$e$ ( $\times 10^{-3}$ )	$i$ (deg)	$P_{orb}$ (d)
Styx	0.60	5.2	1.00	198	42,656	2.263	5.787	0.809	20.16155
Nix	45.0	20.0	1.34	487	48,694	2.583	2.036	0.133	24.85463
Kerberos	1.0	6.0	1.11	405	57,783	3.065	3.280	0.389	32.16756
Hydra	48.0	20.0	1.24	661	64,738	3.434	5.862	0.242	38.20177

<sup>a</sup>Based on published analyses of the mass ( $m_s$  in units of  $10^{18}$  g), radius ( $r_s$ ), density ( $\rho_s$  in units of  $\text{g cm}^{-3}$ ), Hill radius ( $r_H$ ), semimajor axis ( $a$ ), orbital eccentricity ( $e$ ) and inclination ( $i$ ), and orbital period ( $P_{orb}$  Brozović et al. 2015; Stern et al. 2015; Weaver et al. 2016; Nimmo et al. 2017; McKinnon et al. 2017).

Table 2. Survivor fraction for  $n$ -body calculations<sup>a</sup>

Orbit	Satellites	Tracer Mass	$a_0/a_{PC}$	$f_s$	Time Scale
Prograde	No	No	1.00–1.50	0.00	10 Myr
Prograde	No	No	1.45–2.10	0.29	10 Myr
Prograde	No	No	1.95–2.65	0.90	10 Myr
Prograde	No	No	2.60–3.25	1.00	10 Myr
Retrograde	No	No	1.00–1.50	0.20	10 Myr
Retrograde	No	No	1.45–2.10	0.98	10 Myr
Retrograde	No	No	1.95–2.65	1.00	10 Myr
Retrograde	No	No	2.60–3.25	1.00	10 Myr
Polar	No	No	1.00–1.50	0.00	10 Myr
Polar	No	No	1.45–2.10	0.00	10 Myr
Polar	No	No	1.95–2.65	0.02	10 Myr
Polar	No	No	2.60–3.25	0.10	10 Myr
Prograde	Yes	No	1.60–2.10	0.19	10 Myr
Prograde	Yes	No	2.10–2.60	0.02	10 Myr
Prograde	Yes	No	2.40–3.00	0.05	10 Myr
Prograde	Yes	No	2.80–3.40	0.05	10 Myr
Prograde	Yes	No	3.20–4.00	0.43	10 Myr
Polar	Yes	No	1.60–2.10	0.00	10 Myr
Polar	Yes	No	2.10–2.60	0.00	10 Myr
Polar	Yes	No	2.40–3.00	0.21	10 Myr <sup>b</sup>
Polar	Yes	No	2.80–3.40	0.14	10 Myr <sup>c</sup>
Polar	Yes	No	3.20–4.00	0.60	10 Myr <sup>d</sup>
Prograde	Yes	Yes	1.76–2.02	0.10	100 Myr <sup>e</sup>
Prograde	Yes	Yes	2.48–2.54	0.10	100 Myr <sup>f</sup>
Prograde	Yes	Yes	3.29–3.36	0.21	100 Myr <sup>g</sup>
Prograde	Yes	Yes	3.84–3.97	0.96	100 Myr <sup>h</sup>
Polar	Yes	Yes	2.67–2.80	0.39	100 Myr
Polar	Yes	Yes	3.00–3.09	0.00	100 Myr
Polar	Yes	Yes	3.71–3.91	1.00	100 Myr

<sup>a</sup>The first column lists the initial sense of the orbits for systems of massless tracers (‘No’ in column three) or one low mass satellite (‘Yes’ in column three) with the range of semimajor axes in column four. Calculations have the Pluto–Charon binary as the central mass, with (‘Yes’ in column two) or without (‘No’ in column two) the four small satellites. The survivor fraction  $f_s$  (length of the simulation) is listed in column five (six).

<sup>b</sup>After 20 Myr, the survivor fraction is 0.18

<sup>c</sup>After 20 Myr, the survivor fraction is 0.08

<sup>d</sup>After 20 Myr, the survivor fraction is 0.57

<sup>e</sup>After 150 Myr, the survivor fraction is 0.03

<sup>f</sup>After 150 Myr, the survivor fraction is 0.10

<sup>g</sup>After 150 Myr, the survivor fraction is 0.14

<sup>h</sup>After 150 Myr, the survivor fraction is 0.90

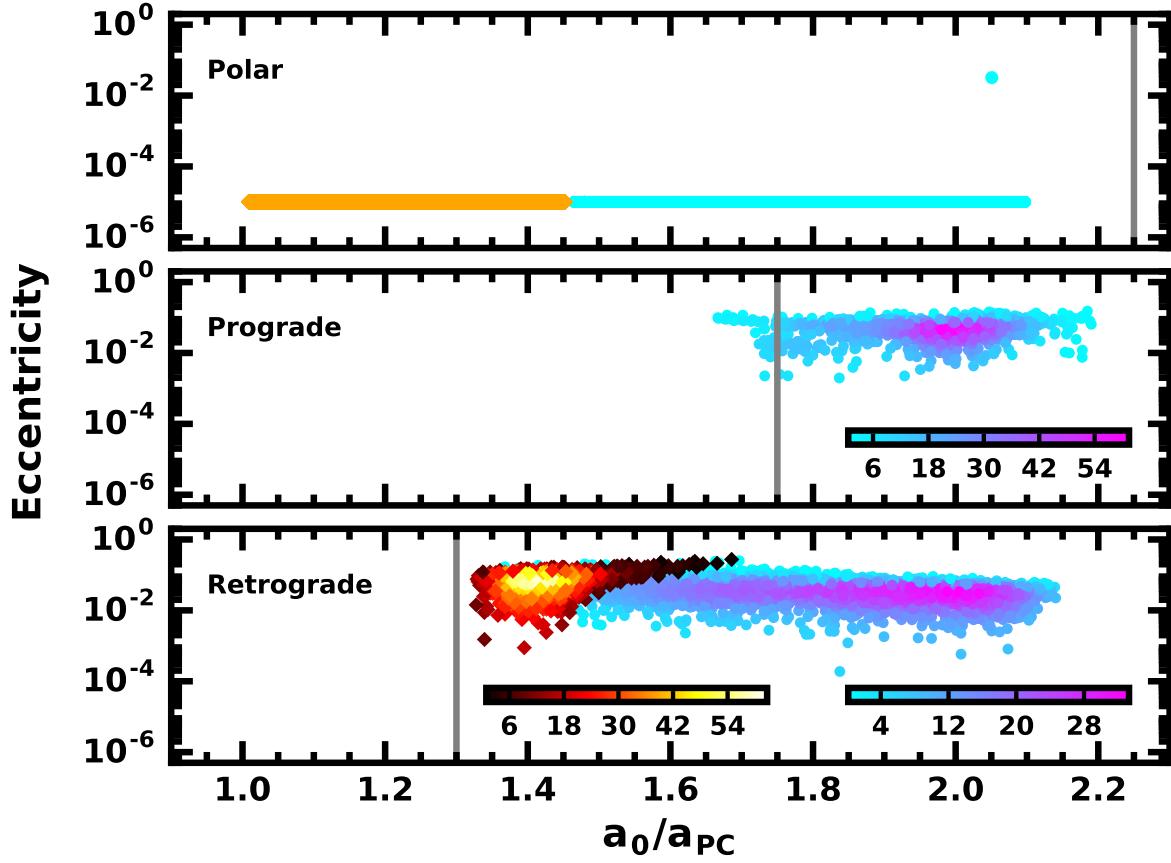


Fig. 1.— Distribution of semimajor axis  $a$  and eccentricity  $e$  for surviving massless test particles polar (upper panel), prograde (middle panel), or retrograde (lower panel) orbits around the Pluto–Charon binary. In the top panel, horizontal orange and cyan lines plot  $(a_0, e_0)$  for each particle. Although we omit these data in other panels for clarity, other calculations have identical  $e_0$ . After 1–2 Myr of evolution, only one test particle with  $(a, e) \approx (2.05, 0.01)$  survives on a polar orbit. In the middle and lower panels, the colors of points within clouds at  $e \approx 0.01$  indicate the density of survivors after 1–2 Myr, as indicated by the colorbars below each cloud. Among test particles with  $a_0 = 1.0\text{--}1.5 a_{PC}$  ( $a_0 = 1.5\text{--}2.1 a_{PC}$ ), the color ranges from dark red (cyan) for low density to orange (light purple) for intermediate density to bright yellow (magenta) for high density. Vertical grey lines indicate the approximate minimum  $a$  for stable orbits from Doolin & Blundell (2011). Although there are no co-rotating survivors with  $a_0 \approx 1.0\text{--}1.5 a_{PC}$  in the middle panel, survivors with larger  $a_0$  cluster at  $a \approx 2 a_{PC}$  and have a negligible density close to the expected minimum stable  $a$ . Retrograde survivors in the lower panel cluster at  $1.4 a_{PC}$  ( $a_0 \approx 1.0\text{--}1.5 a_{PC}$ ) and at  $2.0 a_{PC}$  ( $a_0 \approx 1.5\text{--}2.1 a_{PC}$ ). The minimum  $a$  for both sets lies just outside the limit of Doolin & Blundell (2011).

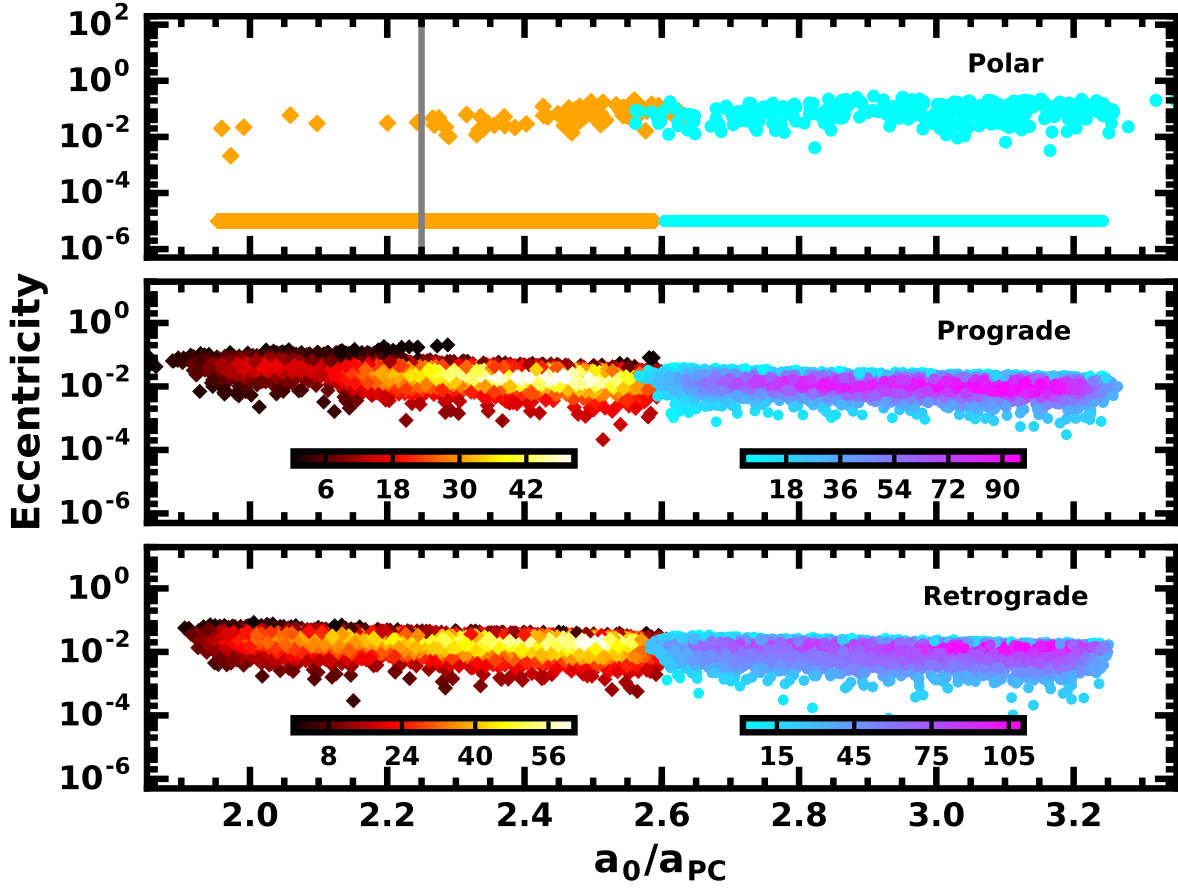


Fig. 2.— As in Fig. 1 for test particles with  $a_0 \approx 2.0$ – $3.2$ . Prograde and retrograde survivors lie in clouds where the typical  $e$  declines slowly with  $a$ . Few survivors on polar orbits lie inside the vertical grey line, which indicates the minimum stable  $a$  of Doolin & Blundell (2011).

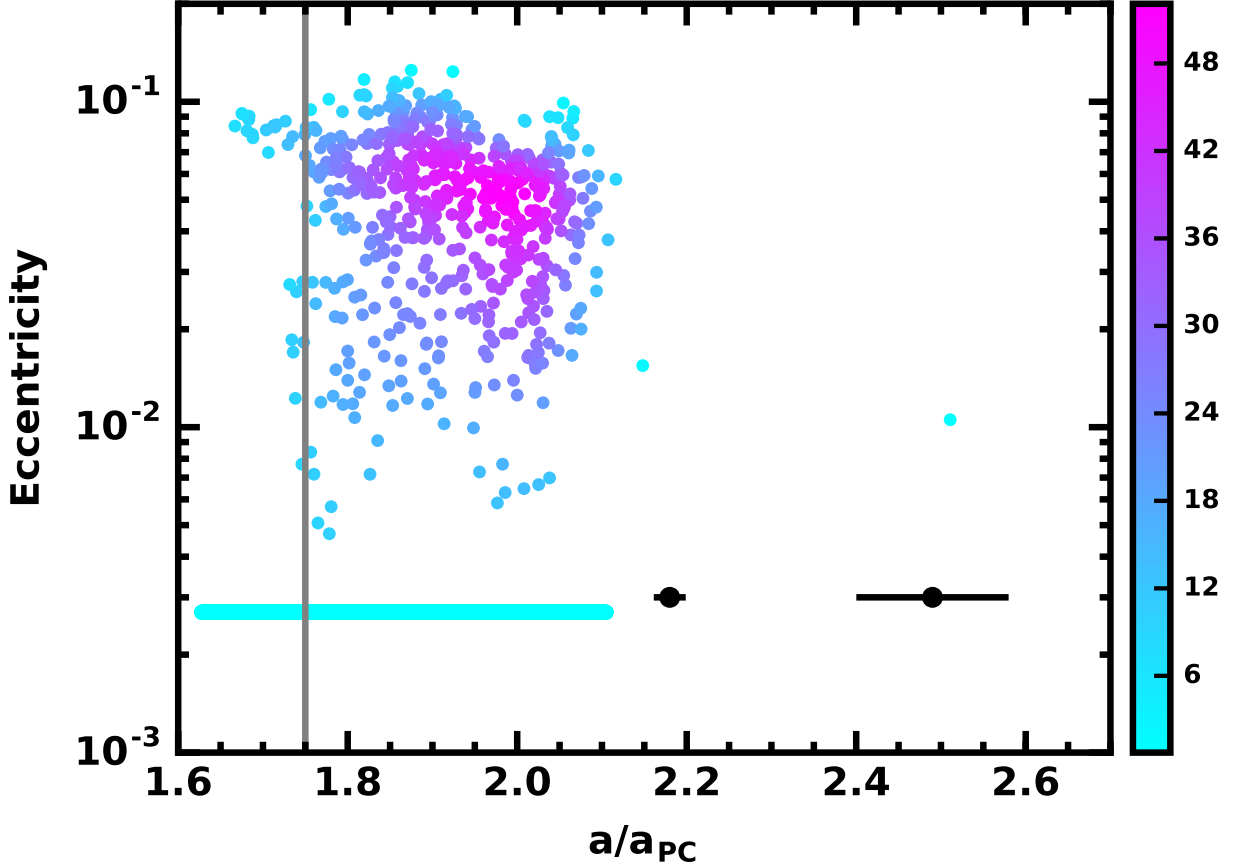


Fig. 3.— Distribution of  $a$  and  $e$  for surviving prograde test particles orbiting with the Pluto–Charon satellites after 10 Myr. The vertical grey line indicates the position of the innermost stable orbit from Doolin & Blundell (2011). Black points plot the positions of the Pluto–Charon satellites; horizontal lines extending from each point have half-width  $\delta a = 2\sqrt{3}r_H$ . Cyan points at  $e \approx 3 \times 10^{-3}$  indicate the initial range of  $a$  for massless tracers co-rotating with the Pluto–Charon binary. Smaller points represent the survivors after 10 Myr of dynamical evolution. Colors of points within the cloud at  $a \approx 1.8$ – $2.1 a_{PC}$  indicate the density of survivors, ranging from low (cyan) to intermediate (purple) to high (magenta) as indicated by the colorbar at the right of the plot. Inside  $a \approx 1.7$ – $1.8 a_{PC}$ , a handful of survivors will become unstable on time scales of  $\lesssim 10$  Myr. Outside this limit, survivors are strongly clustered at  $a \approx 1.9$ – $2.0 a_{PC}$  with a broad range of  $e$ .

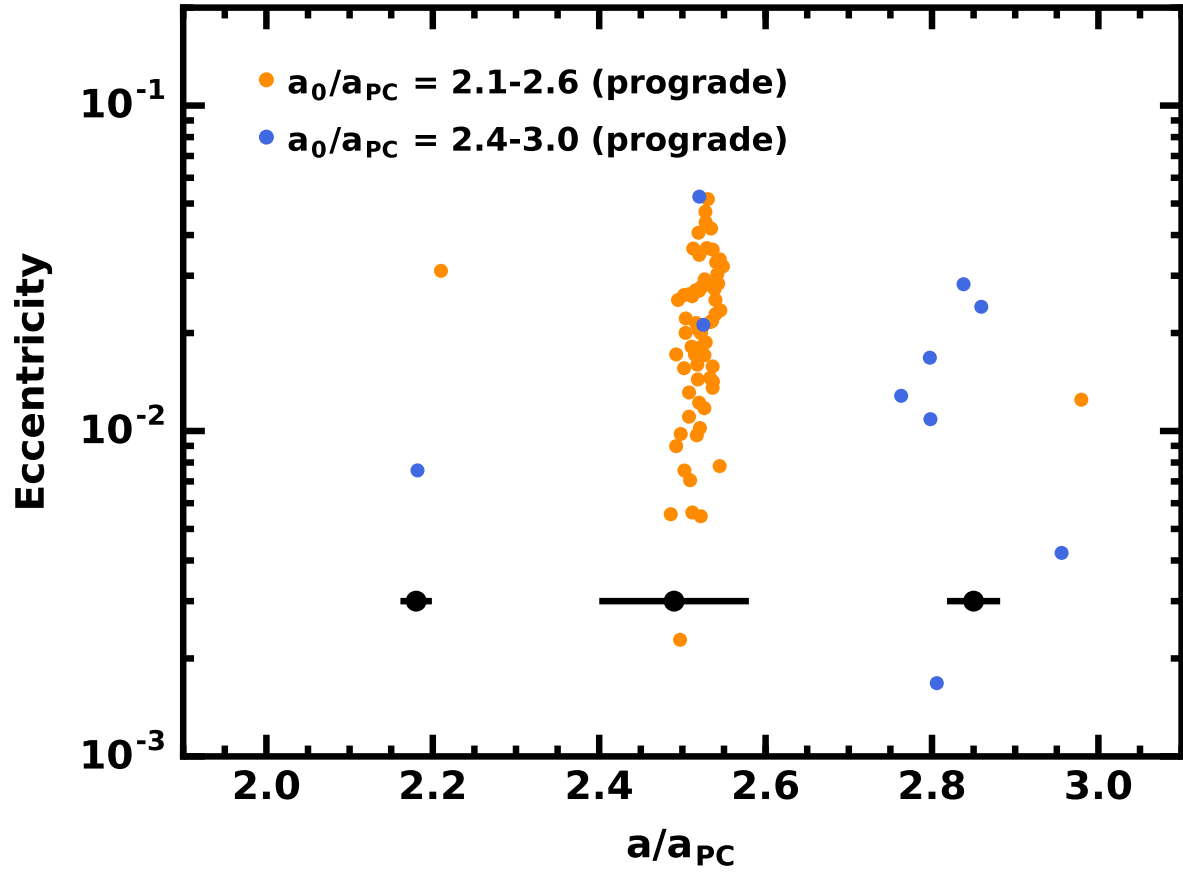


Fig. 4.— As in Fig. 3 for prograde test particles with  $a_0 = 2.1-2.6 a_{PC}$  (orange points) or  $a_0 = 2.4-3.0 a_{PC}$  (cyan points). After 10 Myr, few test particles survive.

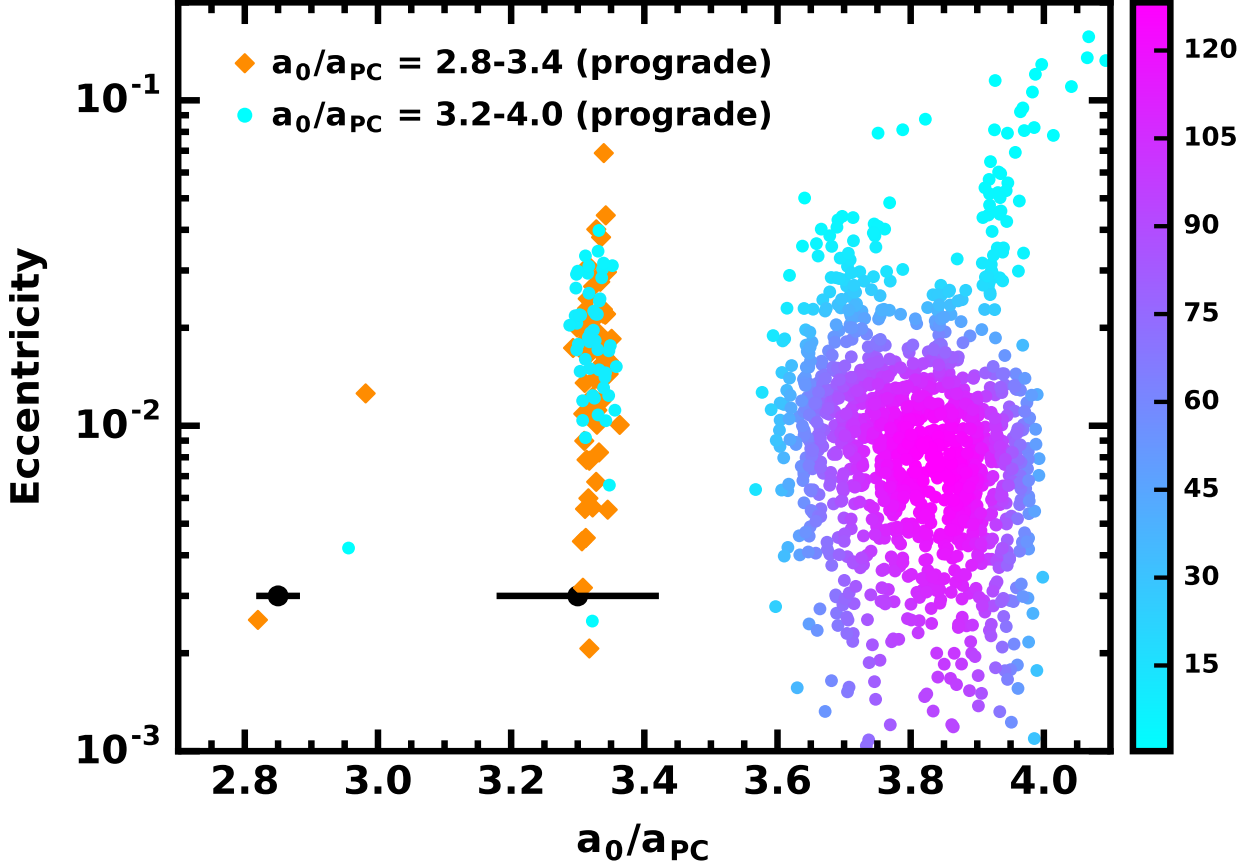


Fig. 5.— As in Fig. 3 for test particles with  $a_0 = 2.8-3.4 a_{PC}$  (orange points) or  $a_0 = 3.2-4.0 a_{PC}$  (cyan points). Colors of points within the cloud at  $a \gtrsim 3.55 a_{PC}$  indicate the density of survivors, ranging from low (cyan) to purple (intermediate) to magenta (high) as indicated by the colorbar to the right of the plot. Inside  $a \approx 3.55 a_{PC}$ , a handful of survivors will become unstable on time scales of  $\lesssim 100$  Myr. Thus, there are no stable orbits inside  $3.55 a_{PC}$ . Outside this limit, survivors are strongly clustered at  $a \approx 3.8 a_{PC}$  with a broad range of  $e$ . Within this group, the high  $e$  objects likely become unstable on time scales of 100–200 Myr.

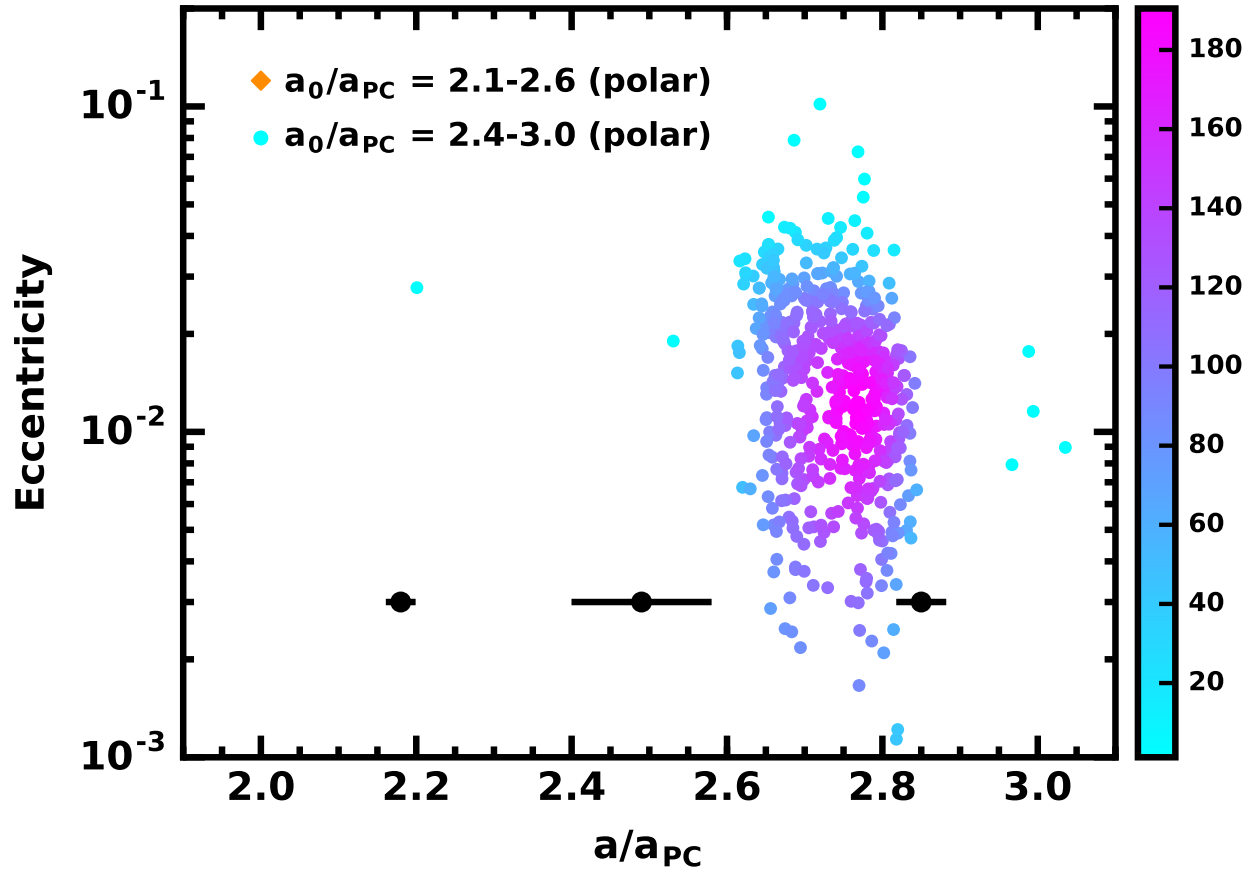


Fig. 6.— As in Fig. 4 for test particles on polar orbits. The few survivors remaining after 10 Myr of evolution are likely to be ejected after 100–200 Myr.

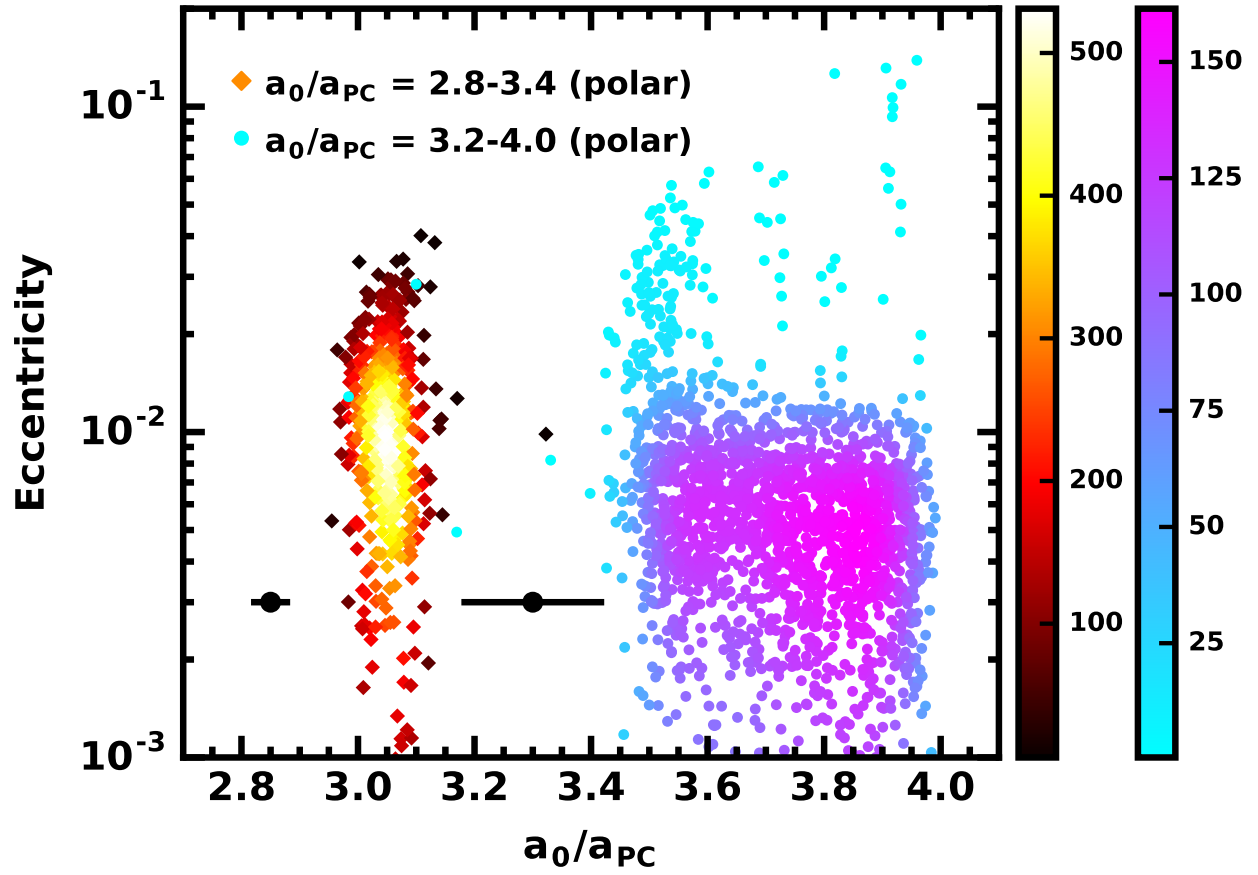


Fig. 7.— As in Fig. 6 for particles with larger  $a_0$ .

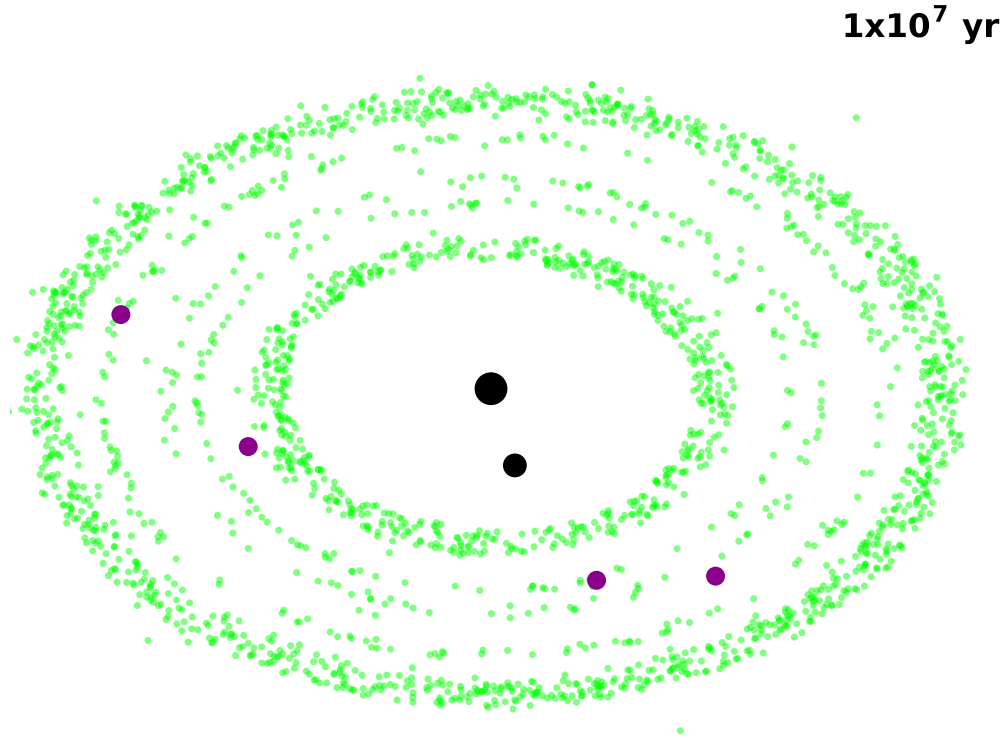


Fig. 8.— Positions of Pluto-Charon (large black dots), the four small satellites (purple dots), and surviving prograde, massless tracers (small green dots) after 10 Myr of dynamical evolution. The system is viewed at an inclination angle of  $45^\circ$  relative to the orbital plane. Most survivors lie just inside the orbit of Styx or outside the orbit of Hydra. Several tracers orbit within the co-rotation zones of Nix or Hydra. A time-lapse animation illustrates the loss of massless tracers with time.

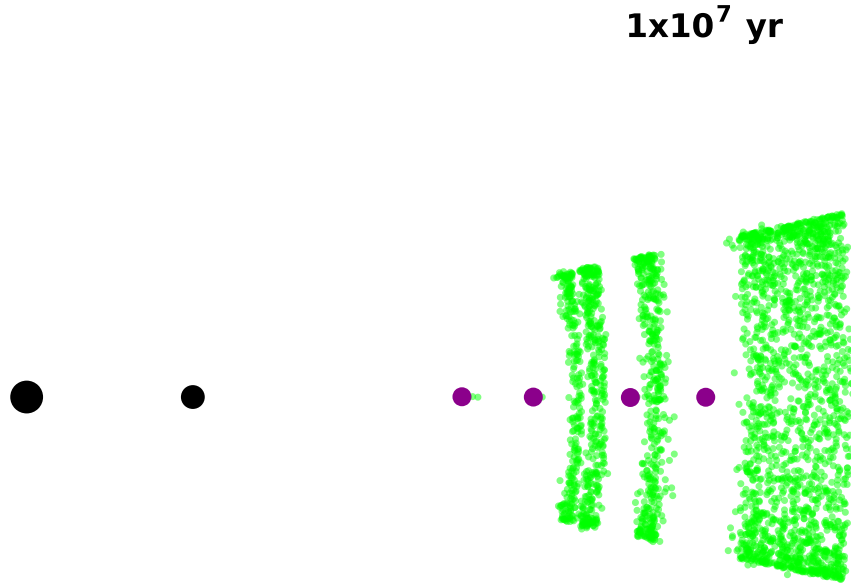


Fig. 9.— As in Fig. 8 for tracers on polar orbits. The view is in the orbital plane, plotting the semimajor axis  $a$  on the  $x$ -axis and the  $z$  distance from the orbital plane on the  $y$ -axis. Most survivors lie just outside the orbit of Hydra. Some tracers survive between the orbits of Nix–Kerberos and the orbits of Kerberos–Hydra. Tracers on polar orbits do not survive inside the orbit of Nix. A time-lapse animation illustrates the loss of massless tracers with time.

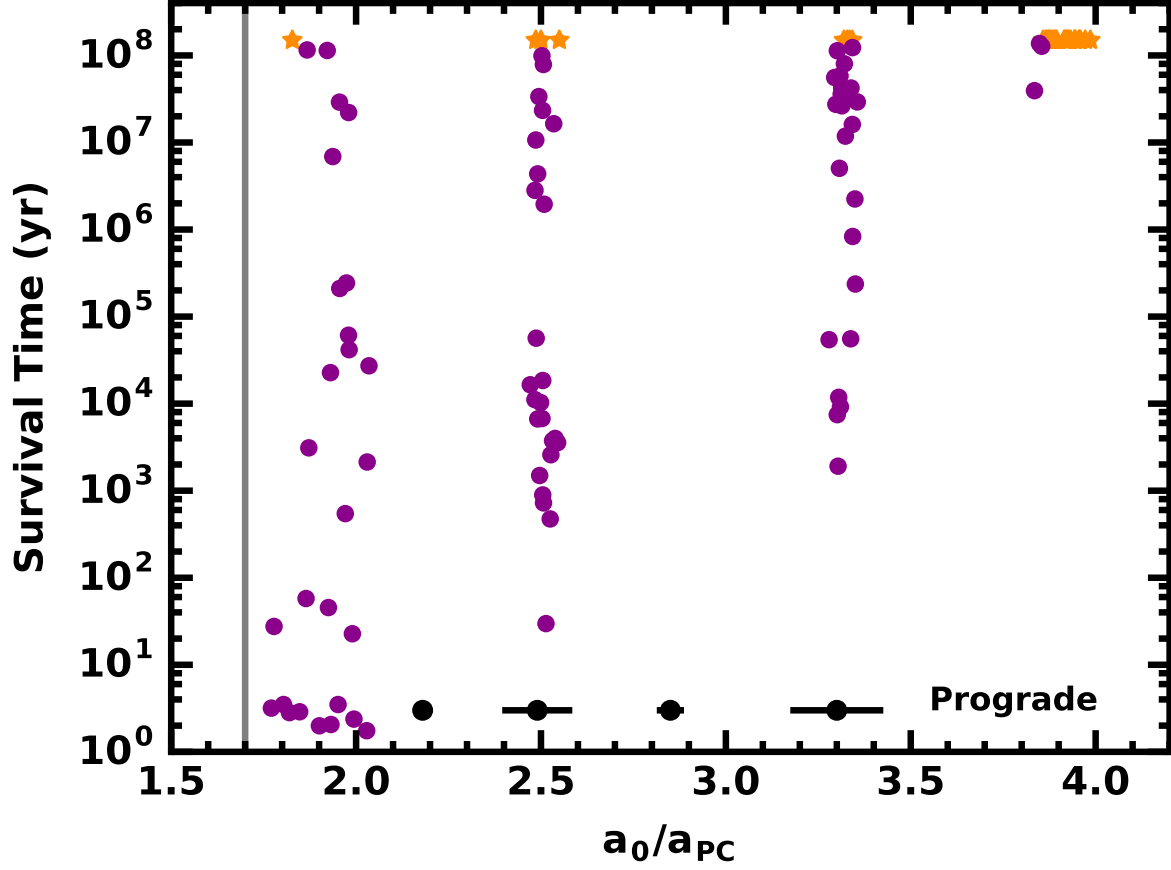


Fig. 10.— Survival time of massive satellites ( $r = 2$  km;  $m = 4 \times 10^{16}$  g) as a function of initial semimajor axis. Purple points: ejected satellites; orange stars: upper limits. Initial orbits are selected from the survivors of test particles placed in nearly circular orbits with  $a_0 = 2.1\text{--}2.6 a_{PC}$  (Fig. 3, orange points),  $a_0 = 2.8\text{--}3.4 a_{PC}$  (Fig. 4, orange points), and  $a_0 = 3.2\text{--}4.0 a_{PC}$  (Fig. 4, magenta points).

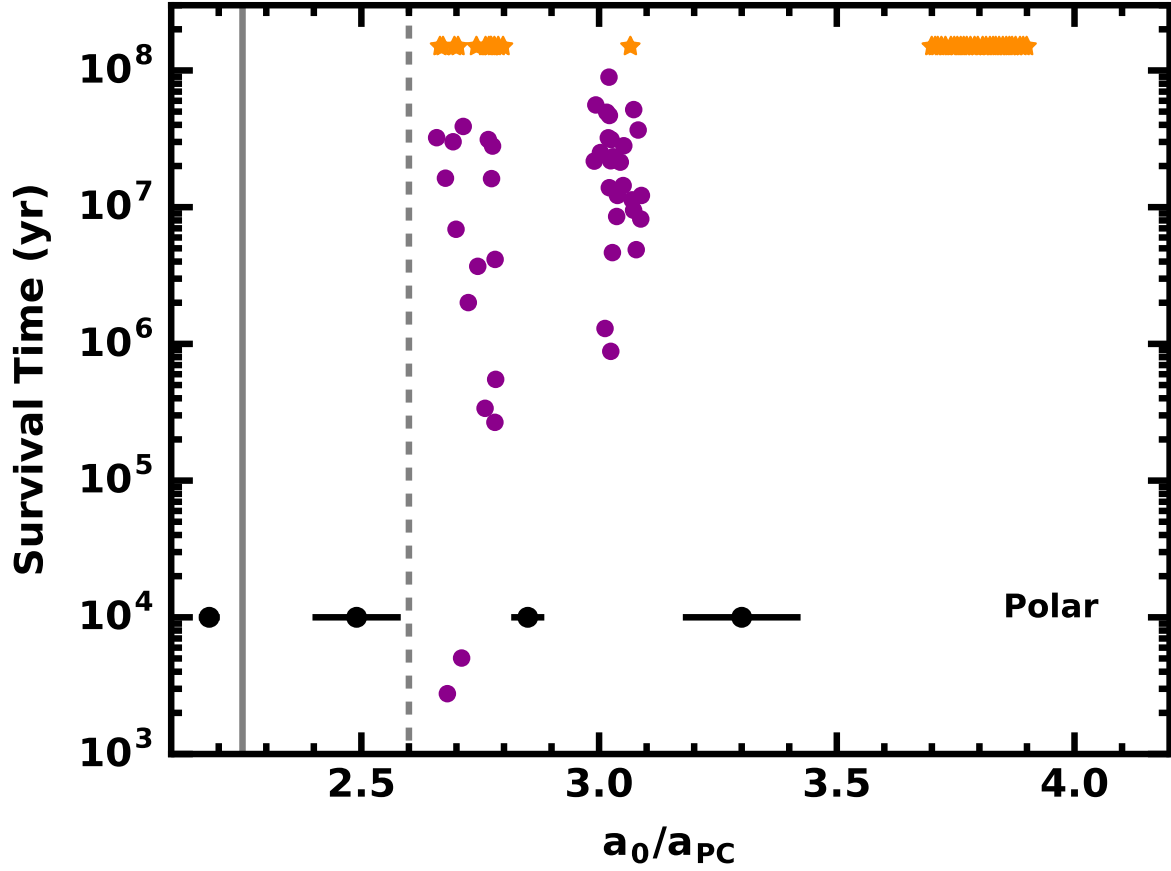


Fig. 11.— As in Fig. 10 for massive satellites ( $r = 2$  km;  $m = 4 \times 10^{16}$  g) on polar, circumbinary orbits. Initial orbits are selected from the survivors of test particles placed in nearly circular orbits with  $a_0 = 2.6$ – $2.85 a_{PC}$  (Fig. 6, orange points),  $a_0 = 2.95$ – $3.1 a_{PC}$  (Fig. 7, orange points), and  $a_0 = 3.7$ – $3.9 a_{PC}$  (Fig. 7, magenta points).

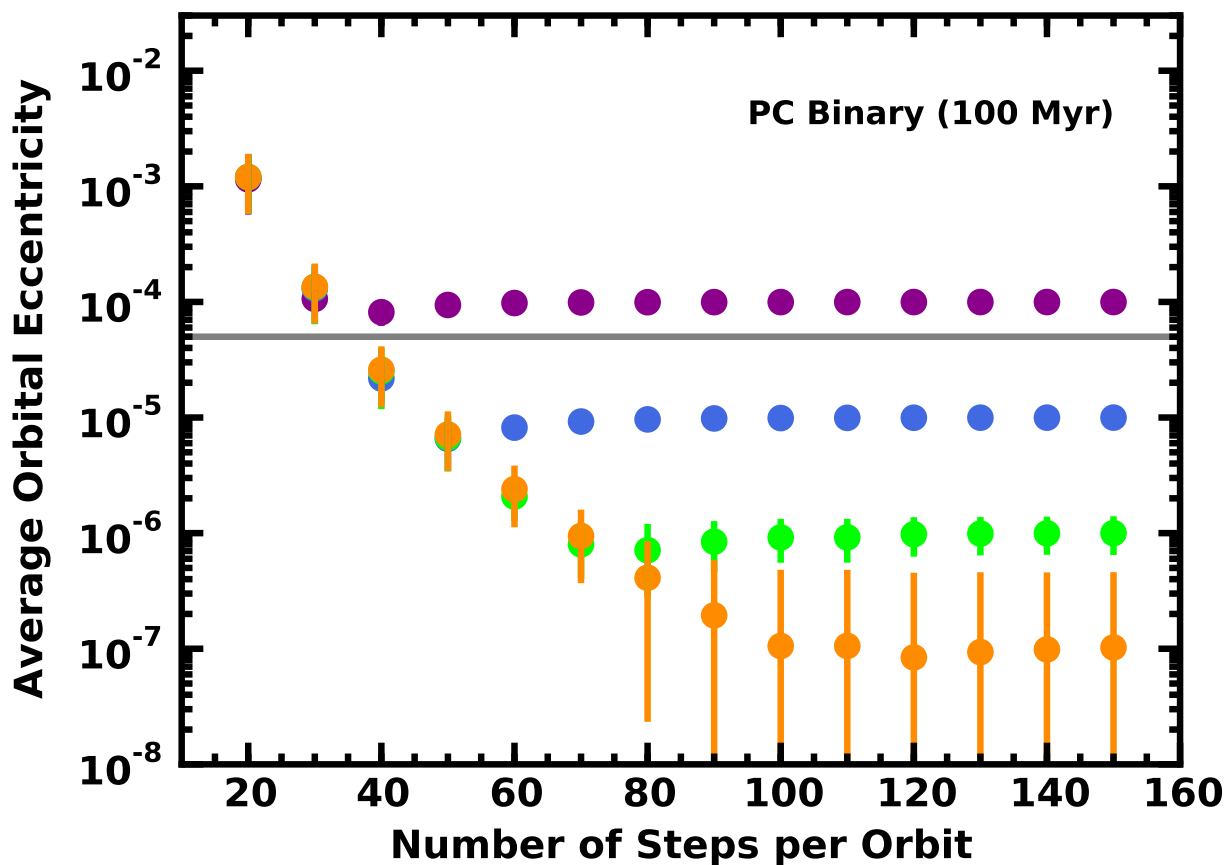


Fig. 12.— Average eccentricity (symbols) and standard deviation (bars) of the Pluto–Charon binary over 100 Myr of evolution as a function of  $N$  the number of symplectic steps per binary orbit. Colors indicate the input eccentricity:  $e_0 = 10^{-4}$  (purple),  $e_0 = 10^{-5}$  (blue),  $e_0 = 10^{-6}$  (green), and  $e_0 = 10^{-7}$  (orange). Calculations with  $N \geq 40$  maintain  $e$  near or below the measured  $e = 5 \times 10^{-5}$  indicated by the horizontal grey line. Smaller  $N$  generates orbital  $e$  much larger than the observed  $e$ . The larger standard deviation for  $e \approx 10^{-7}$  is due to round-off error in our method for deriving  $e$  from the orbital position and velocity.